Electronic Supplementary Information

Hot-Excitons Harvesting via Through-Space Single-Molecule Based White-Light Emission and Optical Waveguides

Debasish Barman[a] Mari Annadhasan,[b] Rajadurai Chandrasekar[b*] and Parameswar Krishnan Iyer[a,c*]

[a]Department of Chemistry, Indian Institute of Technology Guwahati, Guwahati-781039, India

[b]School of Chemistry, and Centre for Nanotechnology, University of Hyderabad, Gachibowli, Prof. C. R Rao Road, Hyderabad, 500046 India

[c]Centre for Nanotechnology, Indian Institute of Technology Guwahati, Guwahati-781039, India

*e-mail: pki@iitg.ac.in

*e-mail: r.chandrasekar@uohyd.ac.in

Contents **Page no.**

1. Materials

Benzothiazole, 1,1'-(5-hydroxy-1,3-phenylene)bis(ethan-1-one), carbazole, 1,3-dibromopropane, 1,4-dibromobutane, 1,5-dibromopentane, 1,6-dibromohexane, sodium hydride, potassium hydroxide, potassium iodide, potassium carbonate and glycerol were purchased from Sigma-Aldrich and used as such without further purification**.** All the solvents used like dimethylsuphoxide, acetone, chloroform and hexane were purified prior to use according to the standard protocol and stored in molecular sieves.

2. Measurements

2.1. Structural Characterization:

All the reactions were carried out in oven dried (~100 °C) round bottom flasks under argon atmosphere unless otherwise mentioned. The ^{1}H and ^{13}C NMR spectra were recorded by using deuterated solvents ($CDCl_3$) in Bruker 600 MHz NMR spectrometer. Chemical shifts (δ) are expressed relative to the resonances of the residual non-deuterated solvent for ^{1}H [$CDCl_3$: ^{1}H (δ) = 7.26 ppm], and ^{13}C [$CDCl_3$:^{13}C(δ) = 77.0 ppm]. Absolute values of the coupling constants are given in Hertz (Hz), regardless of their sign. Multiplicities are abbreviated as singlet (s), doublet (d), doublet of doublets (dd), triplet (t), multiplet (m), and broad (br).

2.2. Compounds Purification:

High-performance liquid chromatogram (HPLC) spectra were recorded from Shimadzu UFLC system. Before running, each sample was purified through 0.22 μm filter to remove any aggregates. The flow rate was fixed at 1.0 mL/min, the injection volume was 20 μL and each sample was run for 20 min. The absorption wavelength used was set at 300 nm. 100 % percent of acetonitrile was used as the running buffer.

2.3. Optical Characterization:

The fluorescence and absorption spectra were measured with PerkinElmer, Model Lambda-25 spectrometer and Horiba-Fluoromax4 with Varian Cary Eclipse spectrometer respectively. The absolute quantum yields were measured by using the Horiba Fluoromax (Jobin Yvon equipped with Integrating sphere) absolute quantum yield spectrometer. The time-resolved fluorescence lifetimes were investigated with the time-resolved fluorescence studies were performed using an Edinburgh Life Spec II instrument. Temperature-dependent (77K-300K) PL and lifetime measurements were carried out using a liquid nitrogen-cooled optical cryostat (Optistat, Oxford Instruments) attached to an Edinburgh FSP-920 instrument.

2.4. Morphology Visualization:

The morphology and crystallinity of the PMMA doped BT2OxCz (x=3, 4, 5, & 6) were examined by scanning electron microscopy (FESEM) (Zeiss, Model: Sigma-300). Spincoated thin film samples were gold-sputtered under vacuum to achieve a thin layer of conductive gold coating on the micro/nano crystalline samples. Atomic force microscopy (AFM) analysis were performed drop-casted sample over silicon substrate, in AFM, Asylum Cypher, Oxford Instruments.

All digital pictures were taken with a canon power shot SX420 IS digital camera.

2.5. Single crystal X-ray diffraction (XRD) data:

Single-crystal structures of BT2O3Cz, and BT2O6Cz were obtained on X-ray diffractometer on Agilent. The single crystal x-ray diffractometer (SC-XRD) is equipped with Mo X-ray source (Mova), CCD detector (Eos), Oxford cryo system (80-500K) and crystal AlisPRO software and Autochem softwares. SCXRD data were collected at 293 K. All the crystal structures were solved by SHELXT with direct methods. All of the non-hydrogen atoms were located by SHELXT directly and refined anisotropically by SHELXL2018 with least squares methods.[1] The revised data have been deposited with the Cambridge Crystallographic Data Center (CCDC) (accession codes CCDC **1969742**, and **1969743**). The stacking structure and intermolecular interactions of the BT2O3Cz and BT2O6Cz were analyzed via Murcury and Materials Studio software. The powder X-ray diffraction measurements of the powder and thin films were performed using a Rigaku SmartLab X-ray diffractometer where copper Kα (λ = 1.54 Å) was used as the source with 9 kW power. The XRD patterns for the 2θ range of 5°−50° were measured at the scan rate 0.3°/s.

2.6. Transient absorption (TA) and Laser-Induced Fluorescence (LIF) measurements:

TA and LIF were performed in an LP980-KS spectrometer configured with a visible PMT detector for kinetic data and an ICCD detector for spectral data acquisition. These detectors were mounted on different ports of the LP980 spectrograph, allowing rapid switching between spectral and kinetic detection. Measurements at 77 K were performed in an Oxford Instruments OptistatDN cryostat placed in the sample chamber of the LP980. The cryostat temperature is controlled from the LP980 operating software, L900. During measurements at room temperature, the slides were either mounted inside the cryostat or in a film sample holder (L-F04). Pump pulses at 355 nm were produced by a Litron Nano S 130-10 laser. The pump pulse width

was ~5 ns and its energy was ~20 mJ/pulse. The white-light probe beam was generated by the Xe lamp in the LP980, operating in pulsed mode and producing pulses with a duration of 6 ms. Pumponly and probe-only backgrounds were subtracted automatically by the L900 software when necessary. Some Laser-Induced Fluorescence (LIF) measurements were performed with a 370 nm longpass filter before the emission monochromator to eliminate the interference from scattered pump light on the spectra.

2.7. Confocal Microspectroscopy studies:

The optical experiments of a single microcrystal were carried out on a backscattering mode setup of the Wi-Tec alpha 300 AR laser confocal optical microscope (LCOM) equipped with a Peltier-cooled CCD detector. Using 300 grooves/mm grating BLZ = 750 nm, the accumulation time was adjusted to 30 s and integration time was typically made 0.5 s. Every single spectrum is obtained by ten averaged accumulations. A diode 405 nm laser source were used for excitation. 20x and 40x objectives was used for spectra and image collection, respectively. All the experiments were carried out under ambient conditions.

2.8. General Characterization:

The transition temperatures and associated enthalpy changes were determined by differential scanning calorimeter (Q20 DSC) under nitrogen atmosphere Thermogravimetric analyses (TGA) were carried out with a Mettler-Toledo TGA/SDTA 851e thermogravimetric analyzer in a temperature range of 30-600 °C under nitrogen atmosphere at 5 °C min^{-1} heating rate.

The growth morphologies of BT2O3Cz and BT2O6Cz crystals were calculated by using the Materials Studio software, based on the attachment energy theory.[2] The molecular structure was first optimized on the basis of the experimental crystal structure. The geometric and energy calculations were performed using the Forcite and Morphology modules.

2.9. Computational Studies:

Combined with the SXRD crystal data, the Hirshfeld surfaces, electrostatic potential, and molecular orbital were simulated by CrystalExplorer 3.1.51.[3] The Hirshfeld surfaces and the electrostatic potential (ESP) were mapped with dnorm using STO-3G basis set at the Hartree-Fock theory.[4, 5] Vertical and transitions energies with the highest occupied molecular orbital (HOMO), lowest unoccupied molecular orbital (LUMO), of single-component crystals were calculated by density functional theory (DFT). All DFT and TDDFT calculations[6] in this study were performed by employing the combination of Becke3-Lee-Yang-Parr (B3LYP) hybrid functional and 6-31G(d,p) basis set using the Gaussian 16 package. The calculated

structures, energy level very much close to experimental results. The UV/Vis absorption (Abs) spectra of compounds were simulated based upon the TDDFT data from Gaussian 16.

2.8. Formula used for Lifetime and Solvatochromism Studies:

$$\tau_{av} = \frac{\{(\alpha_1.\tau_1) + (\alpha_2.\tau_2)\}}{(\alpha_1 + \alpha_2)} \qquad Equation\ S1$$

Where τ_{av} is avarage decay time tau's(τ) are decay components and alphas(α) respective amplitudes.

$$\nu_A - \nu_F = \frac{2\Delta f(\mu_E - \mu_G)^2}{hC \quad a^3},\ \Delta f = \frac{\varepsilon - 1}{2\varepsilon + 1} - \frac{n^2 - 1}{2n^2 - 1} \qquad Equation\ S2$$

In which ν_A is the wavenumber of the absorption, ν_F is the wavenumber of the emission, **h** is Planck's constant, **C** is the speed of light, a is the cavity radius and Δf is the orientation polarizability where Δf is defined by the dielectric constant **ε** and the refractive index **n.**

2.9. Excited-State Kinetics: Rate constants related to the excited-state kinetics are obtained fromthe PLQY, lifetime, and fraction of the prompt and delayed components by using reported protocols(equation S3 – S8).[7,8,9]

$$k_P = {}^{1}\!/_{\tau_F} \qquad \textbf{Equation S3}$$

$$k_D = {}^{1}\!/_{\tau_{TADF}} \qquad \textbf{Equation S4}$$

$$k_F = {}^{\phi_F}\!/_{\tau_F} \qquad \textbf{Equation S5}$$

$$\phi = {}^{k_F}\!/_{(k_F + k_{IC})} \qquad \textbf{Equation S6}$$

$$\phi_F = {}^{\kappa_F}\!/_{(k_F + k_{IC} + k_{ISC})} \qquad \textbf{Equation S7}$$

$$k_{RISC} = {}^{k_P k_D}\!/_{(k_P - k_{ISC})} \qquad \textbf{Equation S8}$$

2.10. The correlated color temperature (CCT) values for corresponding color coordinates were calculated using McCamy et al.'s cubic curve equation.[10]

$$T_c = -437n^3 + 3601n^2 - 6861n + 5514.31 \qquad \textbf{Equation S9}$$

$n = (x - 0.3320)/(y - 0.1858)$ and the CCT value for the nearest white light emitting sample was found to be below 5000 K. This range of CCT values indicated that the BT2OxCz systems could be a potential candidate for warm white-light emitting phosphors.

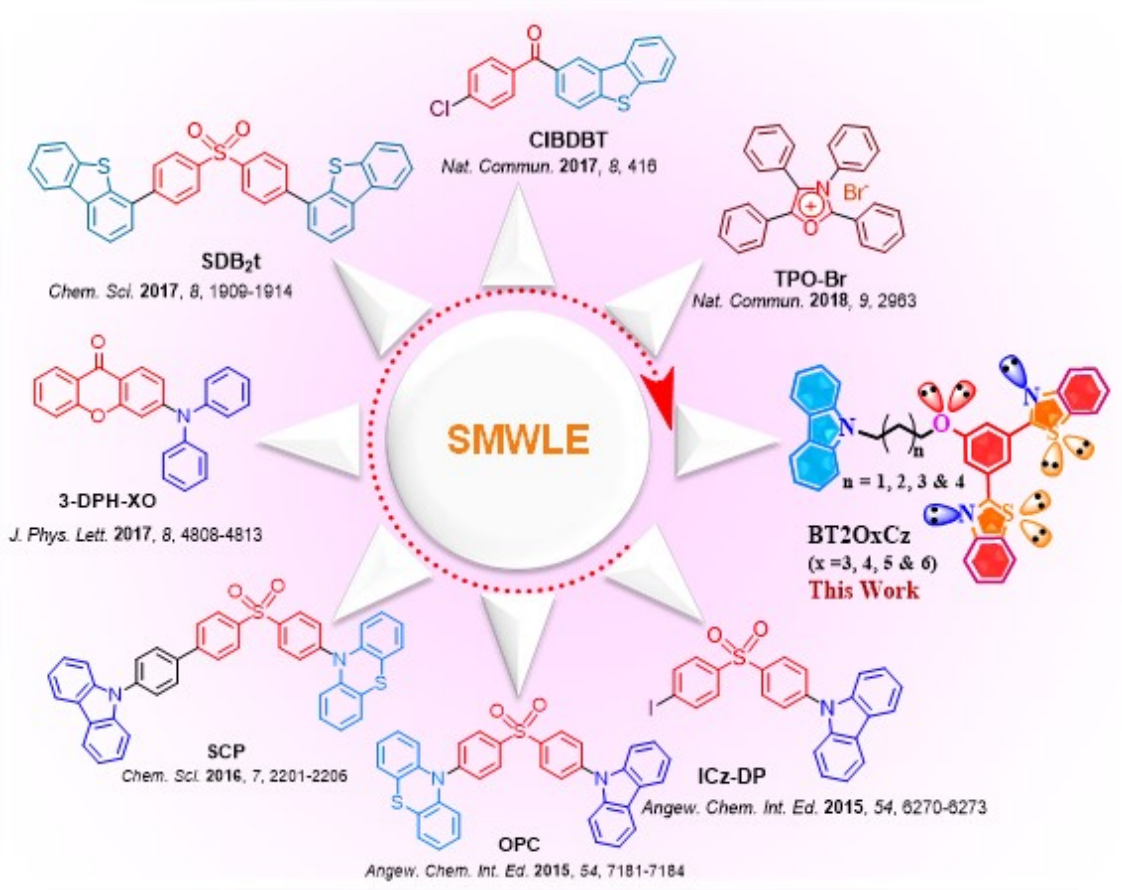

Figure S1. State-of-the-art reported organic single molecule white light emitters (OSMWLEs), in this work, the design of through-space donor-σ-acceptor [BT2OxCz (x= 3, 4, 5 & 6)] derivatives of various alkoxy group connected between 9H-carbazol and di substituted phenyl benzothiazole moiety.

Synthesis and characterizations

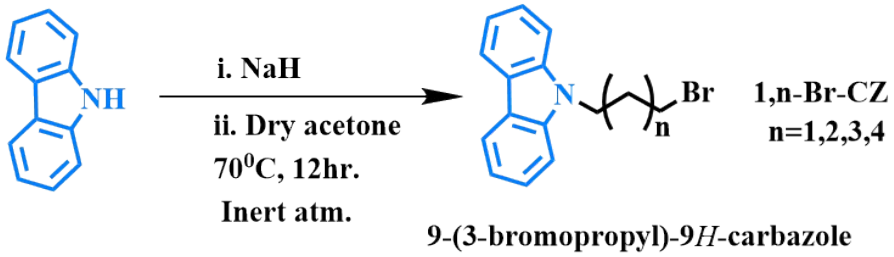

Scheme S1. Synthesis of 1, n-Br-Cz [9-(n-bromalkyl,)-9H-Carbazole] (1,n-BrCz):

Carbazole (1g, 5.98 mmol) was dissolved in dry acetone (about 20 ml) in a 100 ml RB then 287 mg of NaH (11.96 mmol) was added to the solution. With the evolution of H_2 gas, the colorless solution became turbid. After 45 minutes, 1.2 equivalent of dibromo alkane (7.17 mmol) (1, 4- dibromo butane; 1, 5- dibromo pentane; 1, 6- dibromo hexane) was added to the mixture of solution and refluxed at 70 ºC for 12 hours. The turbit solution was turn to clear honey color. Then stopped the reaction and TLC checked, a new intense spot was observed. After that, the solvent was removed with the help of vacuum and the obtained crude solid was worked up with DCM and distilled H_2O followed by brine solution for three times until the base was completely removed from the organic portion and the organic layer was dried over anhydrous Na_2SO_4. The mixture was purified by column chromatography by using silica gel (100-200 mesh size) with hexane/dichloromethane (19:1 v/v) as eluent, colorless solid was obtained. The colorless solids were further recrystallized with 20% DCM: hexane mixture and calculate yield of 90% for all the 1,n- Cz-Br (n= 3,4,5,6) compounds. Further, characterize all the derivatives using ^1H, ^{13}C and HRMS respectively

1, 3-Br-Cz [9-(3-bromopropyl)-9H-Carbazole] : ^1H NMR (600 MHz, CDCl3) δ 8.15 (d, J = 7.8 Hz, 1H), 7.52 (dd, J = 4.0, 1.4 Hz, 2H), 7.29 (ddd, J = 7.9, 5.3, 2.7 Hz, 1H), 4.51 (t, J = 6.6 Hz, 1H), 3.40 (t, J = 6.2 Hz, 1H), 2.47 – 2.43 (m, 1H). ^{13}C NMR (151 MHz, CDCl3) δ 140.37 (s), 125.84 (s), 123.01 (s), 120.43 (s), 119.16 (s), 108.61 (s), 77.26 (s), 77.05 (s), 76.84 (s), 40.94 (s), 31.98 (s), 30.81 (s). HRMS (ESI) peaks of m/z value of (M & M+2) was calculated 288.0388, 290.0367 and observed 288.0389, 290.0373. (**Figure-S1-S3**).

1, 4-Br-Cz [9-(4-bromobutyl)-9H-Carbazole] : ^1H NMR (600 MHz, $CDCl_3$) δ 8.14 (d, *J* = 7.7 Hz, 1H), 7.50 (t, *J* = 7.6 Hz, 1H), 7.43 (d, *J* = 8.2 Hz, 1H), 7.27 (t, *J* = 7.3 Hz, 1H), 4.38 (t, *J* = 7.0 Hz, 1H), 3.41 (t, *J* = 6.5 Hz, 1H), 2.08 (d, *J* = 7.7 Hz, 1H), 1.95 (d, *J* = 8.3 Hz, 1H).

^{13}C NMR (151 MHz, $CDCl_3$) δ 140.28 (s), 125.74 (s), 122.89 (s), 120.45 (s), 118.96 (s), 108.54 (s), 77.26 (s), 77.05 (s), 76.84 (s), 42.18 (s), 33.21 (s), 30.25 (s), 27.68 (s).

HRMS (ESI) peaks of m/z value of (M & M+2) was calculated 302.0544, 304.0524 and observed 304.0561, 304.0545. (**Figure-S4-S6**).

1, 5-Br-Cz [9-(5-bromopentyl)-9H-Carbazole] : ^{1}H NMR (400 MHz, $CDCl_3$) δ 7.99 (d, *J* = 7.8 Hz, 1H), 7.35 (t, *J* = 7.6 Hz, 1H), 7.27 (d, *J* = 8.2 Hz, 1H), 7.12 (t, *J* = 7.4 Hz, 1H), 4.18 (t, *J* = 7.1 Hz, 1H), 3.21 (t, *J* = 6.7 Hz, 1H), 1.75 (ddd, *J* = 11.3, 7.6, 4.7 Hz, 2H), 1.41 (t, *J* = 3.7 Hz, 1H). ^{13}C NMR (101 MHz, $CDCl_3$) δ 140.22 (s), 125.56 (s), 122.74 (s), 120.29 (s), 118.74 (s), 108.45 (s), 77.26 (s), 76.94 (s), 76.63 (s), 42.67 (s), 33.23 (s), 32.35 (s), 28.06 (s), 25.78 (s)

HRMS (ESI) peaks of m/z value of (M & M+2) was calculated 316.0701, 318.0680 and observed 316.0707, 318.0690. (**Figure-S7-S9**).

1, 6-Br-Cz [9-(6-bromohexyl)-9H-Carbazole] : ^{1}H NMR (600 MHz, $CDCl_3$) δ 8.14 (d, *J* = 7.7 Hz, 1H), 7.50 (t, *J* = 7.2 Hz, 1H), 7.43 (d, *J* = 8.2 Hz, 1H), 7.27 (t, *J* = 7.4 Hz, 1H), 4.33 (t, *J* = 7.1 Hz, 1H), 3.38 (t, *J* = 6.7 Hz, 1H), 1.94 – 1.90 (m, 1H), 1.85 – 1.81 (m, 1H), 1.51 – 1.47 (m, 1H), 1.44 – 1.40 (m, 1H). ^{13}C NMR (151 MHz, $CDCl_3$) δ 140.36 (s), 125.62 (s), 122.80 (s), 120.38 (s), 118.77 (s), 108.60 (s), 77.26 (s), 77.05 (s), 76.84 (s), 42.83 (s), 33.80 (s), 32.55 (s), 28.83 (s), 27.92 (s), 26.46 (s).

HRMS (ESI) peaks of m/z value of (M & M+2) was calculated 330.0857, 330.0837 and observed 332.0864, 332.0846. (**Figure-S10-S12**).

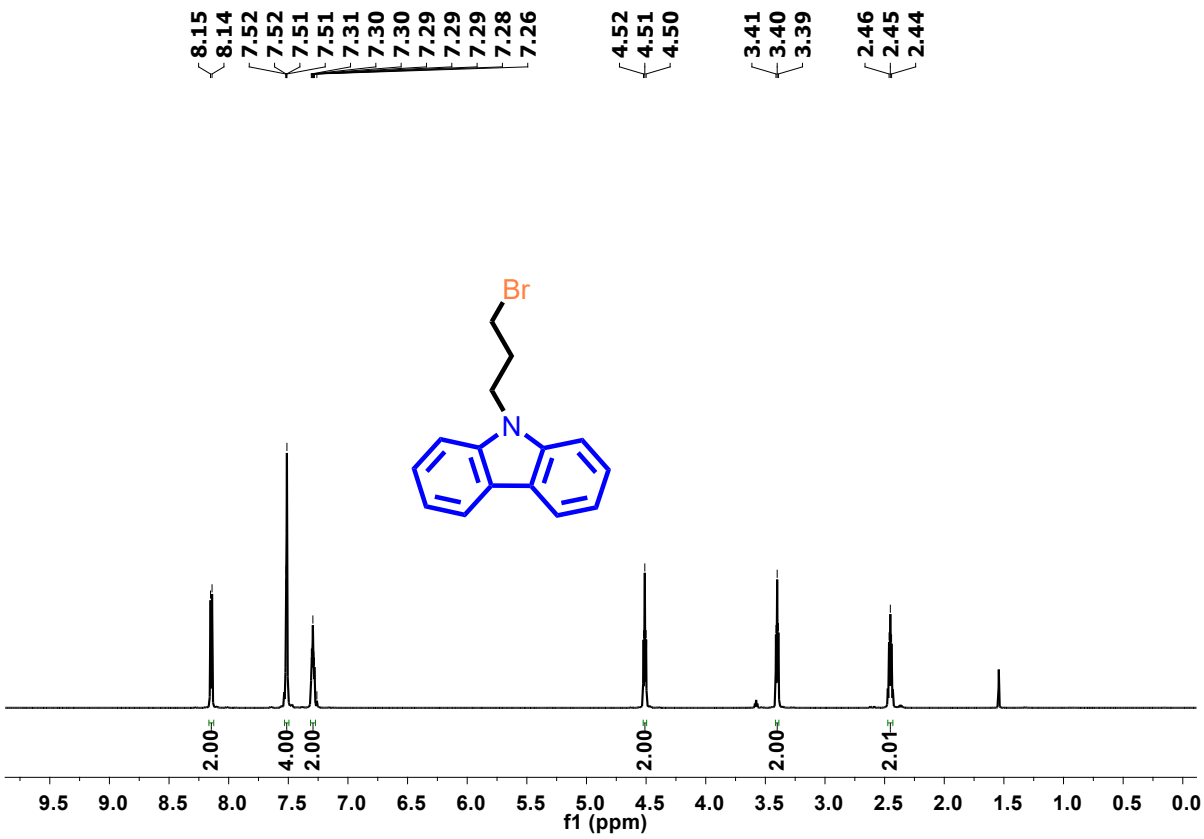

Figure S2. ^{1}H NMR spectra of 1,3-CzBr in $CDCl_3$ at 298K.

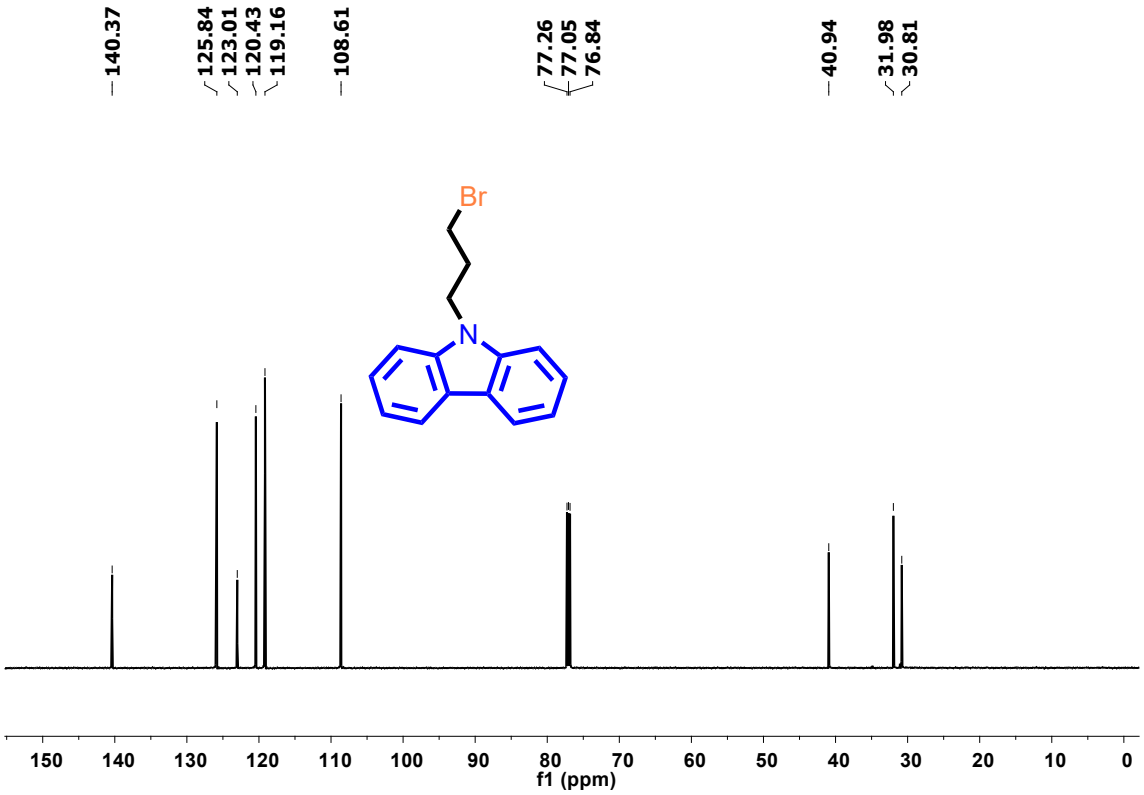

Figure S3. ^{13}C- NMR spectra of 1,3-CzBr in CDCl3 at 298K.

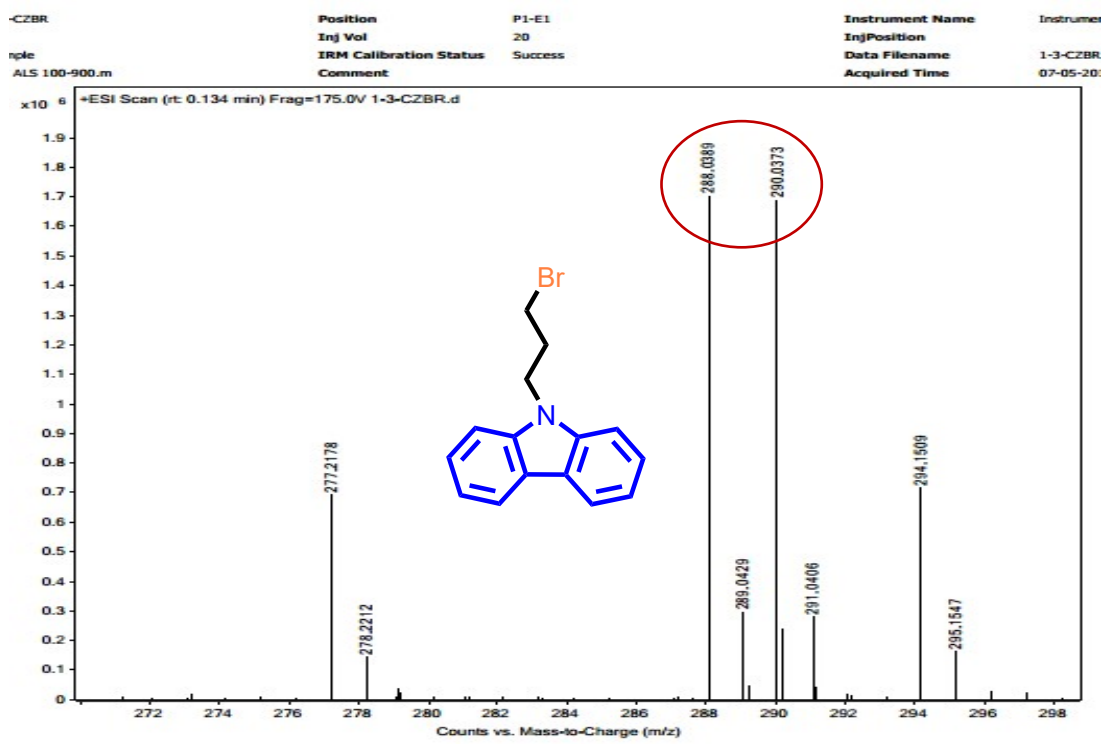

Figure S4. HRMS (ESI) peaks of m/z value for $[1,3\text{-CzBr} + H]^+$ (M & M+2) was calculated 288.0388, 290.0367 and observed 288.0389, 290.0373 at 298K in Acetonitrile solvent.

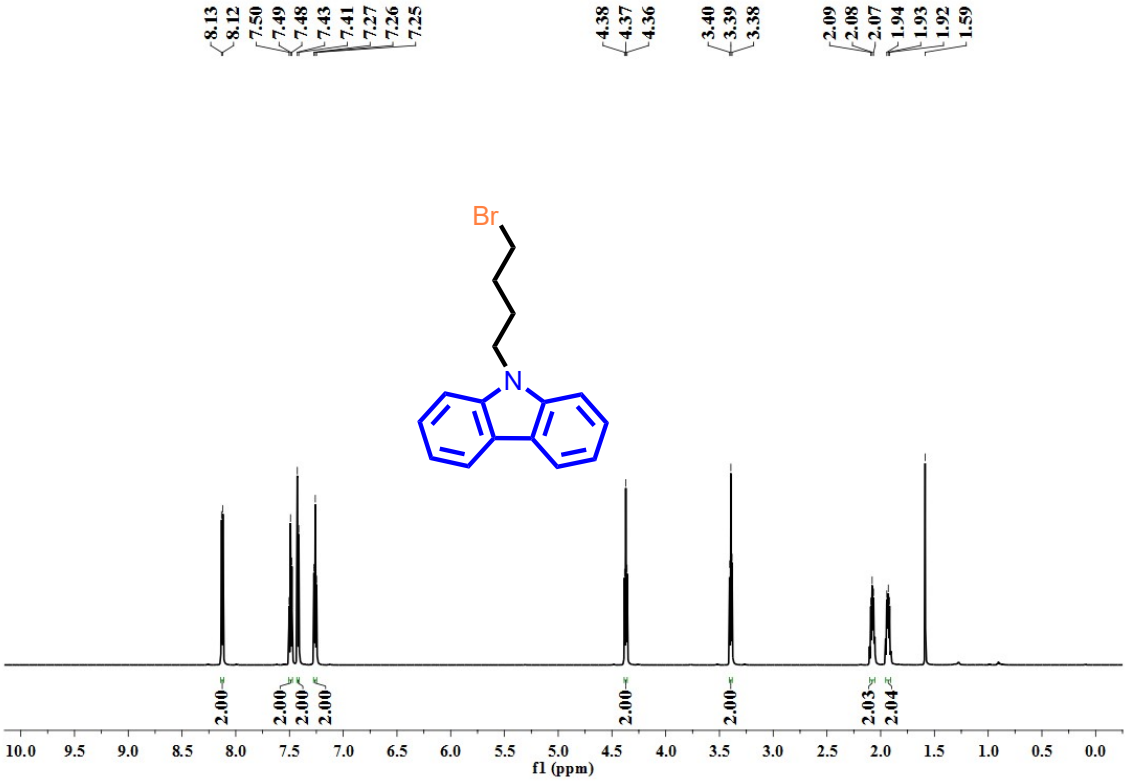

Figure S5. ^{1}H NMR spectra of 1,4-CzBr in $CDCl_3$ at 298K.

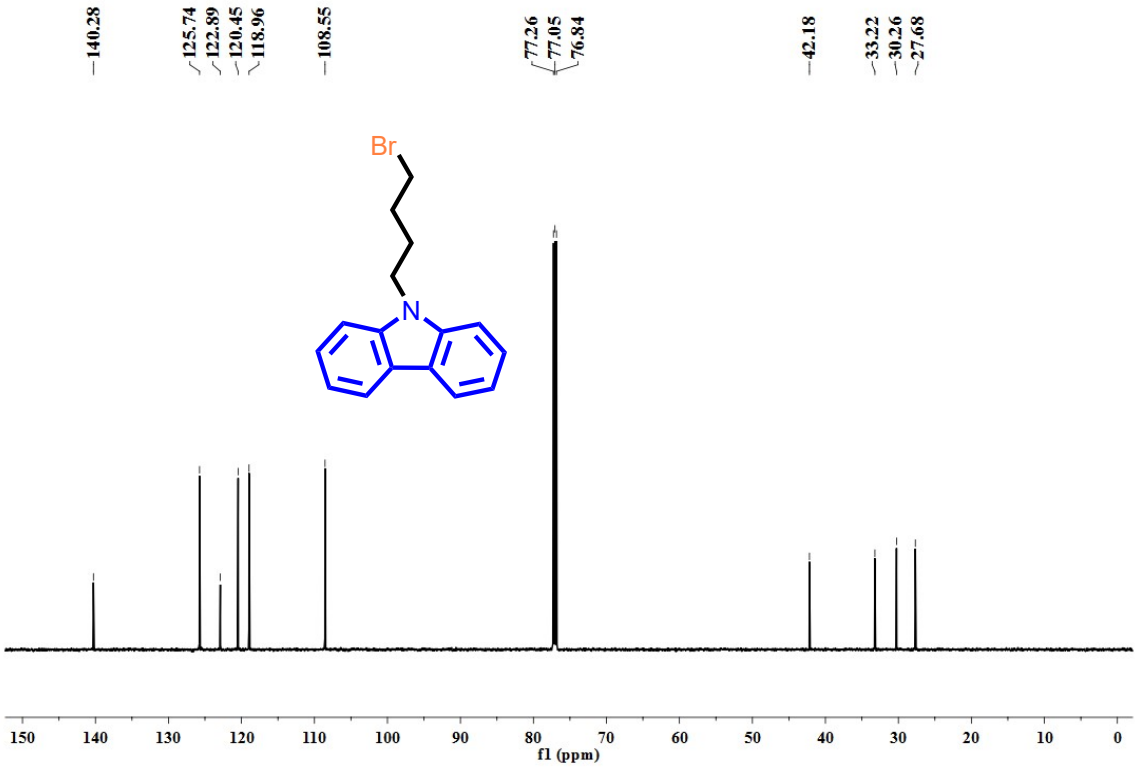

Figure S6. ^{13}C NMR spectra of 1,4-CzBr in $CDCl_3$ at 298K.

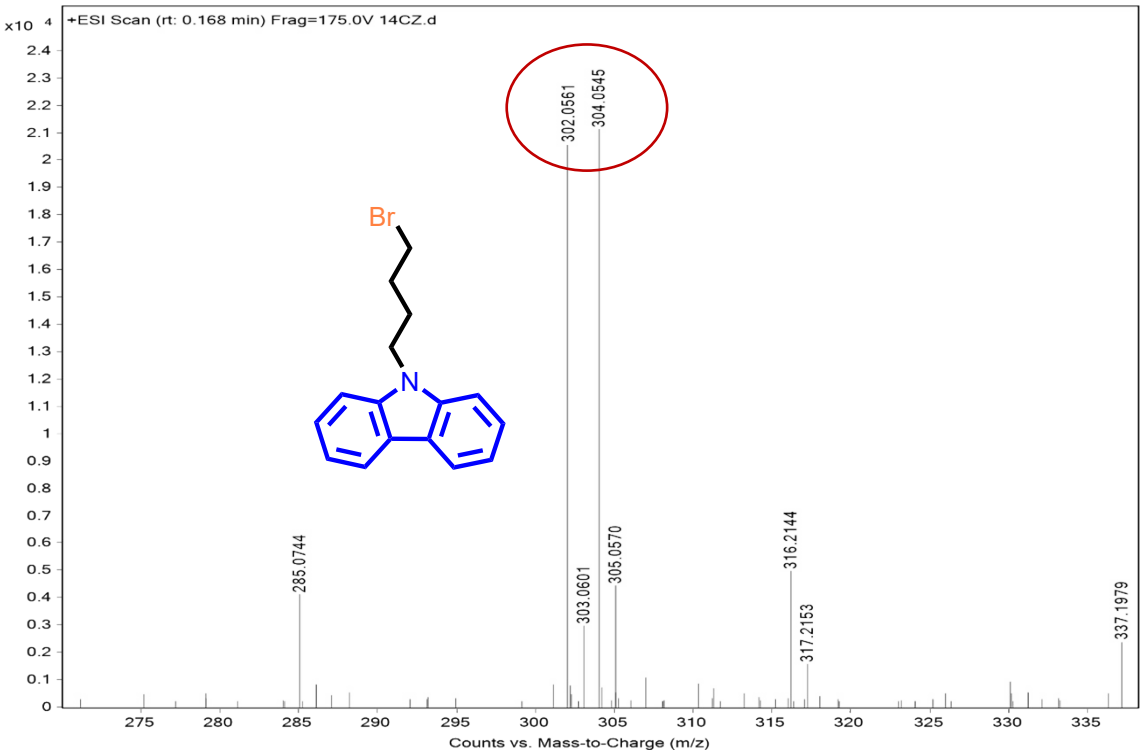

Figure S7. HRMS (ESI) peaks of m/z value for $[1,4\text{-CzBr} + H]^+$ (M & M+2) was calculated 302.0544, 304.0524 and observed 304.0561, 304.0545 at 298K in Acetonitrile solvent.

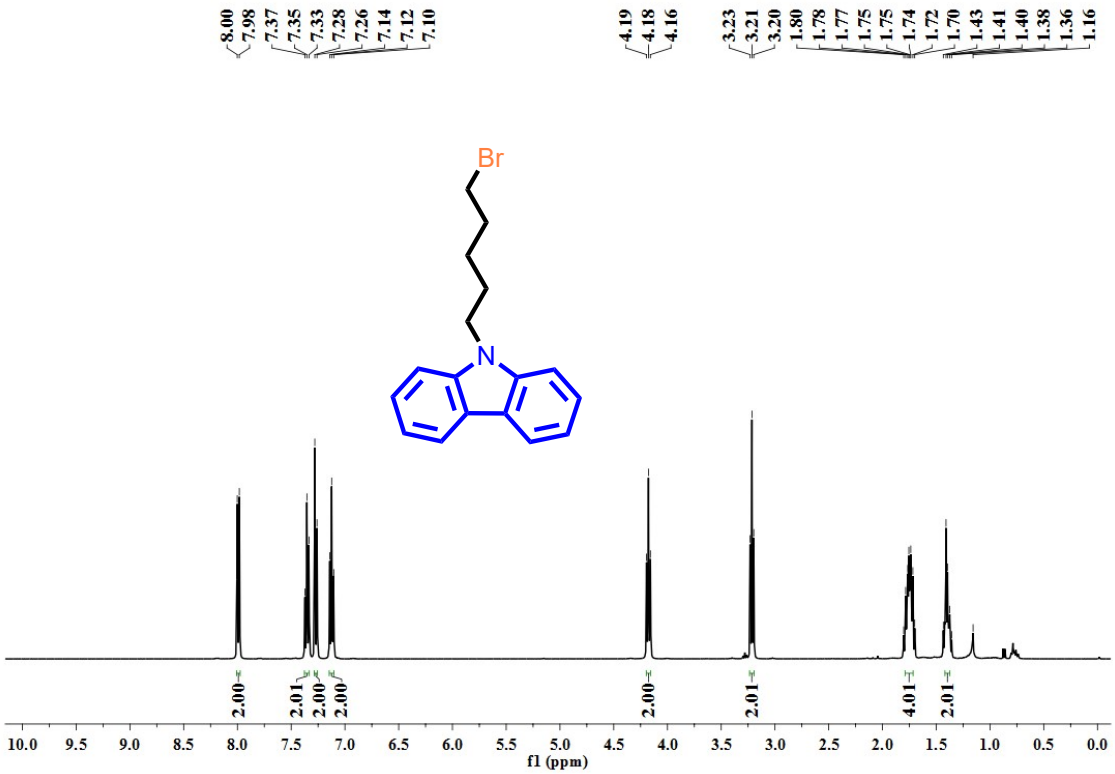

Figure S8. ^{1}H NMR spectra of 1,5-CzBr in $CDCl_3$ at 298K.

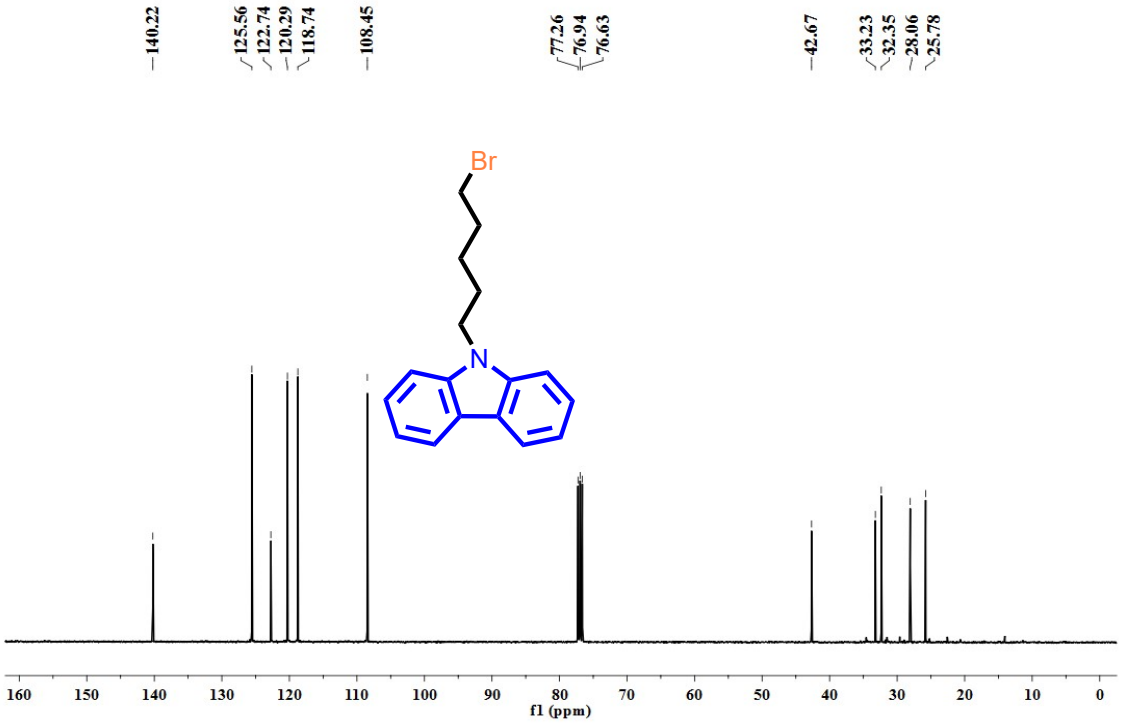

Figure S9. ^{13}C- NMR spectra of 1,5-CzBr-Cz in $CDCl_3$ at 298K.

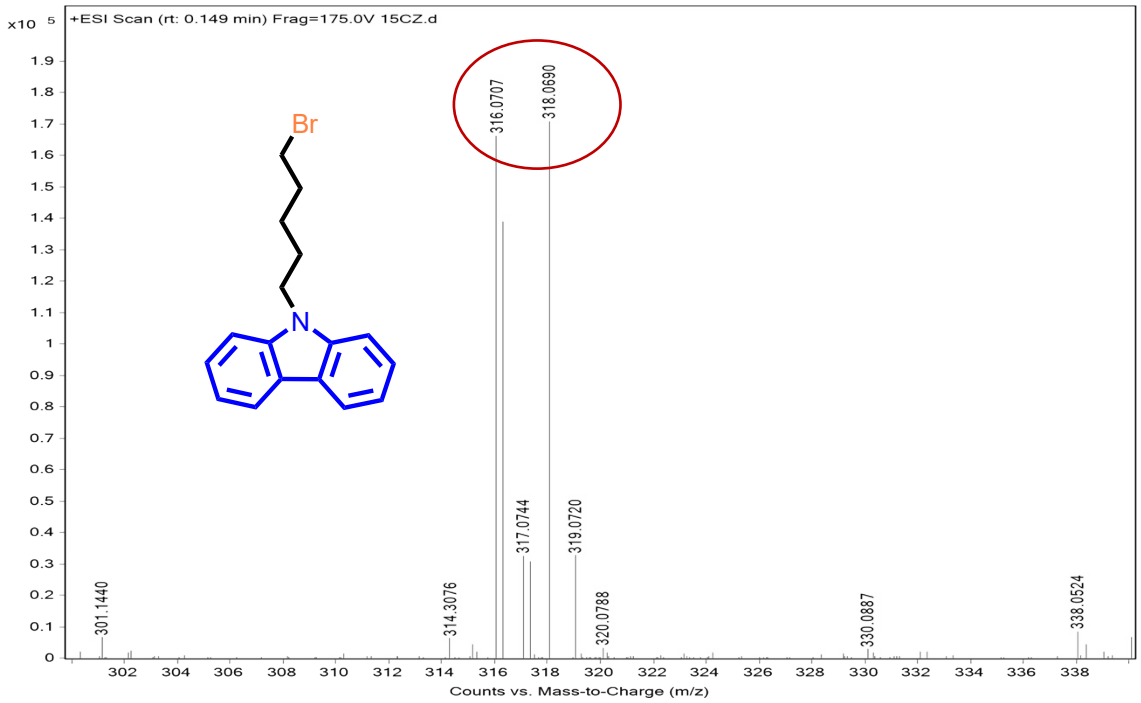

Figure S10. HRMS (ESI) peaks of m/z value for $[1,5\text{-CzBr} + H]^+$,(M & M+2) was calculated 316.0701, 318.0680 and observed 316.0707, 318.0690 at 298K in Acetonitrile solvent.

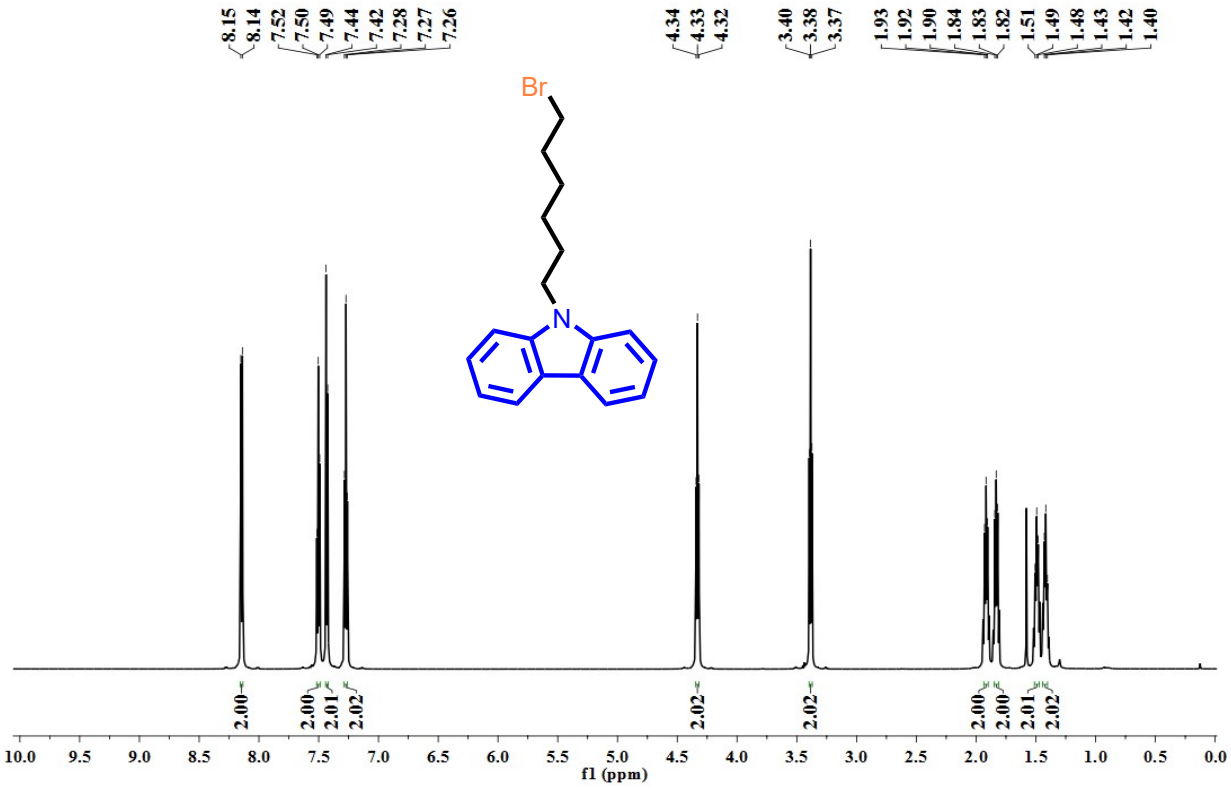

Figure S11. ^1H NMR spectra of 1,6-CzBr in $CDCl_3$ at 298K.

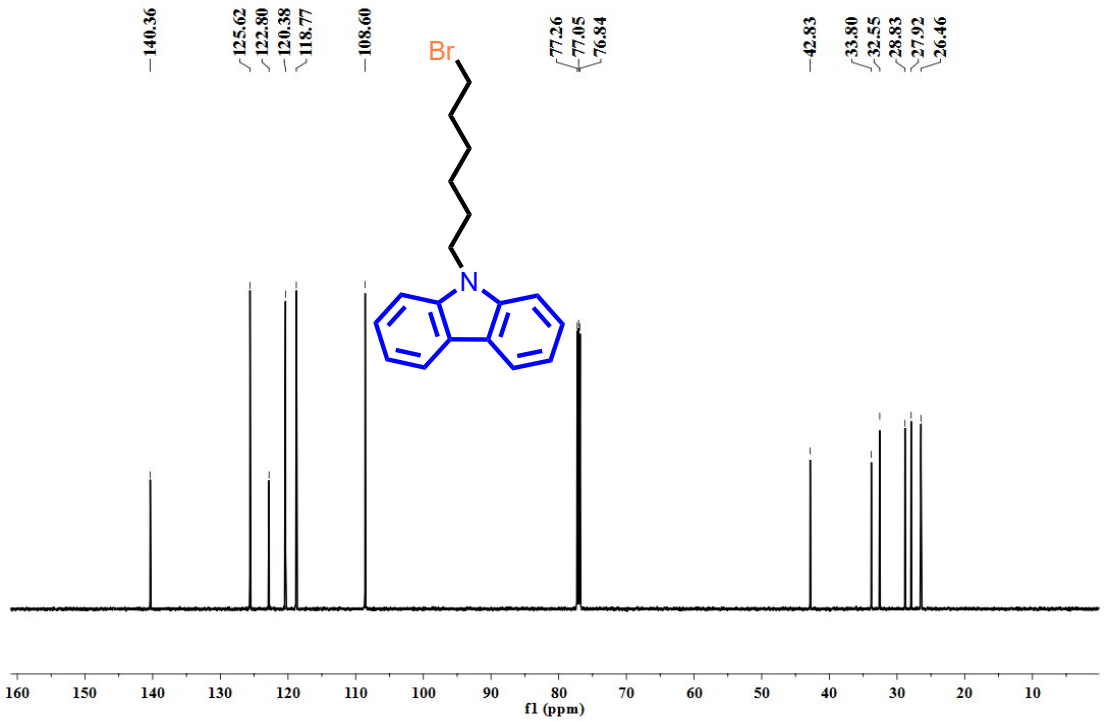

Figure S12. ^{13}C- NMR spectra of 1,6-CzBr-Cz in $CDCl_3$ at 298K.

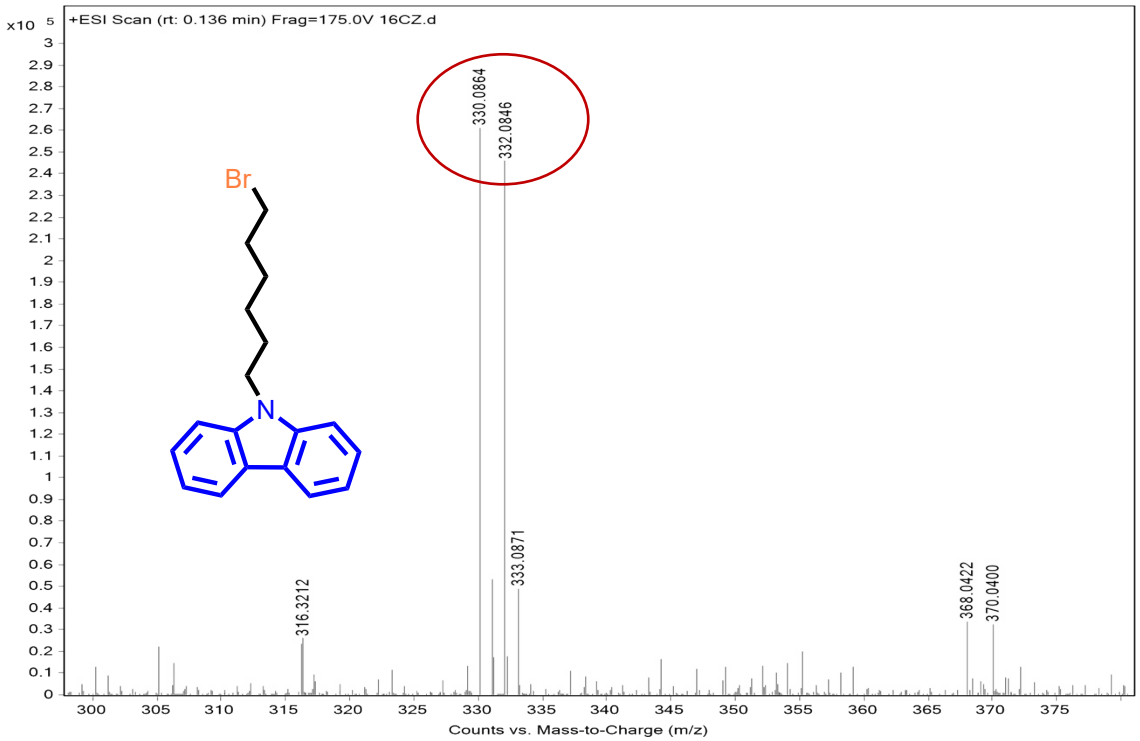

Figure S13. HRMS (ESI) peaks of m/z value for [1,6-CzBr + H]+ ,(M & M+2) was calculated 330.0857, 330.0837 and observed 332.0864, 332.0846 at 298K in Acetonitrile solvent.

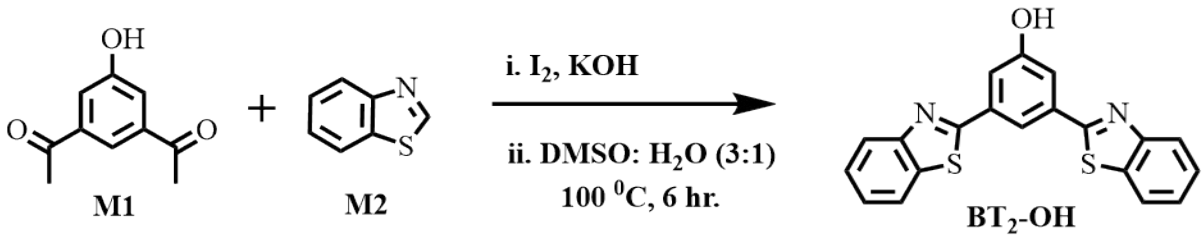

Scheme S2. Synthesis of 3,5-bis(benzothiazol-2-yl)phenol (BT2OH) via in-situ cross coupling.[11]

1,1'-(5-hydroxy-1,3-phenylene)bis(ethan-1-one) (2g, 11.2 mmol), benzothiazole (3g, 22 mmol), iodine (5.6g, 22 mmol) and potassium hydroxide (1.23g, 22 mmol) were taken in DMSO : water (3:1) at room temperature. The mixture was heated up to 100 °C and the completion of the reaction was monitored using analytical TLC technique. After 12 h the reaction mixture was cooled to at room temperature. Then the crude mixture was extracted with ethyl acetate and washed with aqueous sodium thiosulfate solution for several times. Then it was dried over anhydrous Na_2SO_4 and concentrated under reduced pressure. Then the obtained blue solid compound was finally purified recrystallization in methanol and proceed for next step.

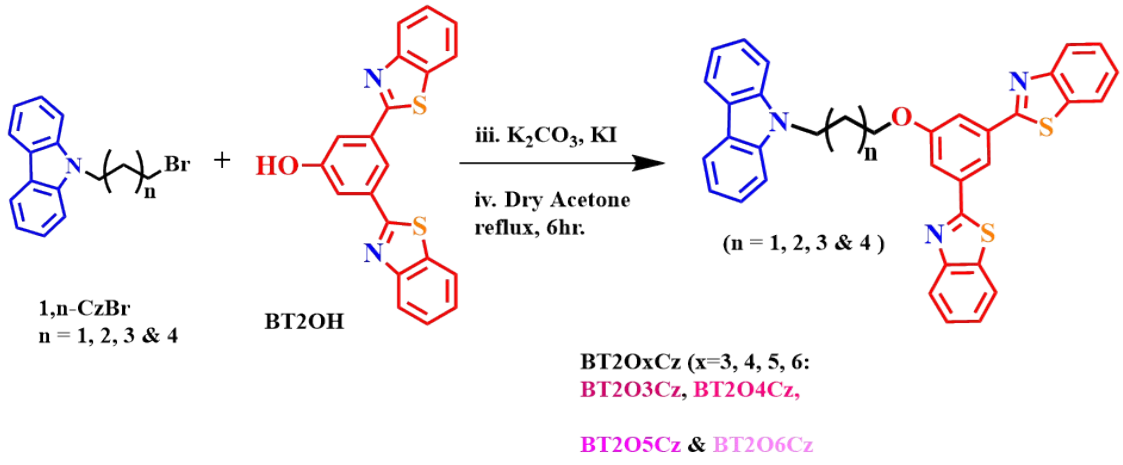

Scheme S3. 2,2'-(5-(3-(9H-carbazol-9-yl)alkoxy)-1,3-phenylene)bis(benzothiazole) [BT2OxCz, x=3,4,5,6]

For this reaction the reagent K_2CO_3 was dried in an oven for overnight in about 200 °C to remove the trace of moistures. In an inert atmosphere (Ag-gas), taking 0.56 mole of BT_2-OH and 154.8 mg of K_2CO_3 in a 100 ml RB followed by the addition of about 15 ml of NMP solvent. The mixture was stirred well on the magnetic stirrer to dissolve the K_2CO_3 at 70 °C After 45 minutes of standing of the solution, adding 1 equiv. of 1, n-Br-Cz (1, 4-Br-Cz = 198.7 mg; 1, 5-Br-Cz = 210 mg 1, 6-Br-Cz = 217.9 mg) to the reaction mixture with a pinch

amount of KI. The reaction was refluxed for 12 hours at 70 °C. In these reactions, the solution for the first time is deep blue color then after 30-45 minutes later, the color of the solution was changing gradually from deep blue to violet to green color. Again, the solution was retained its early color after 12 hours. TLC was checked and the reaction was stopped (TLC solvent was 1:1 v/v DCM: Hexane). The solvent was removed with the help of vacuum RV and the reaction mixture was worked up with DCM and distilled H_2O followed by Brine (NaCl) for several times until the base was removed from the organic portion and the organic layer was dried with anhydrous Na_2SO_4. The residue was purified by silica gel (100-200 mesh) with coulomb chromatography using solvent (Hexane/dichloromethane 19:1 v/v; 9:1 v/v; 5.6:1 v/v with the respect of polarity of the products) as the eluent to obtain a desired product (white color in amorphous state).

2,2'-(5-(3-(9H-carbazol-9-yl)propoxy)-1,3-phenylene)bis(benzothiazole) [BT2O3Cz]:

^{1}H NMR (600 MHz, CDCl3) δ 8.34 (s, 1H), 8.11 (dd, J = 7.7, 4.6 Hz, 4H), 7.95 (d, J = 7.9 Hz, 2H), 7.78 (d, J = 1.2 Hz, 2H), 7.53 (t, J = 7.2 Hz, 2H), 7.49 (d, J = 8.2 Hz, 2H), 7.43 (t, J = 7.6 Hz, 4H), 7.22 (t, J = 7.4 Hz, 2H), 4.64 (t, J = 6.6 Hz, 2H), 4.16 (t, J = 5.5 Hz, 2H), 2.47 – 2.43 (m, 2H). ^{13}C NMR (151 MHz, CDCl3) δ 166.82 (s), 154.00 (s), 140.44 (s), 135.75 (s), 135.22 (s), 126.55 (s), 125.85 (s), 125.58 (s), 123.47 (s), 122.96 (s), 121.76 (s), 120.42 (s), 119.54 (s), 119.06 (s), 115.64 (s), 108.61 (s), 77.26 (s), 77.05 (s), 76.84 (s), 65.37 (s), 39.46 (s), 28.68 (s). HRMS (ESI) peaks of m/z value was calculated 568.1517 and observed 568.1485. (**Figure-S13-S15**).

2,2'-(5-(4-(9H-carbazol-9-yl)butoxy)-1,3-phenylene)bis(benzothiazole) [BT2O4Cz]:

^{1}H NMR (600 MHz, $CDCl_3$) δ 8.34 (s, 1H), 8.14 – 8.12 (m, 4H), 7.96 (d, *J* = 7.9 Hz, 2H), 7.76 (d, *J* = 1.2 Hz, 2H), 7.54 (s, 2H), 7.50 (dd, *J* = 5.6, 4.7 Hz, 4H), 7.44 (s, 2H), 7.27 (d, *J* = 10.7 Hz, 2H), 4.48 (s, 2H), 4.19 (s, 2H), 2.19 (s, 2H), 1.96 (dd, *J* = 13.7, 6.8 Hz, 2H). ^{13}C NMR (151 MHz, $CDCl_3$) δ 166.88 (s), 159.78 (s), 154.01 (s), 140.40 (s), 135.70 (s), 135.23 (s), 126.52 (s), 125.75 (s), 125.54 (s), 123.45 (s), 122.93 (s), 121.76 (s), 120.45 (s), 119.34 (s), 118.91 (s), 115.58 (s), 108.67 (s), 77.26 (s), 77.05 (s), 76.84 (s), 68.15 (s), 42.77 (s), 29.74 (s), 27.04 (s). HRMS (ESI) peaks of m/z value was calculated 582.1674 and observed 582.1686. (**Figure-S16-S18**).

2,2'-(5-((5-(9H-carbazol-9-yl)pentyl)oxy)-1,3-phenylene)bis(benzothiazole) [BT2O5Cz]:

^{1}H NMR (600 MHz, $CDCl_3$) δ 8.35 (s, 1H), 8.14 (dd, *J* = 7.8, 4.0 Hz, 4H), 7.97 (d, *J* = 7.8 Hz, 2H), 7.77 (d, *J* = 1.2 Hz, 2H), 7.56 (t, *J* = 7.6 Hz, 2H), 7.53 – 7.48 (m, 4H), 7.45 (d, *J* = 7.2 Hz, 2H), 7.29 (s, 2H), 4.41 (t, *J* = 7.1 Hz, 2H), 4.17 (t, *J* = 6.2 Hz, 2H), 2.04 (s, 2H), 1.93 (s,

2H), 1.67 (s, 2H).^{13}C NMR (151 MHz, $CDCl_3$) δ 166.96 (s), 159.89 (s), 154.00 (s), 140.40 (s), 135.64 (s), 135.21 (s), 126.52 (s), 125.69 (s), 125.54 (s), 123.43 (s), 122.86 (s), 121.76 (s), 120.41 (s), 119.22 (s), 118.82 (s), 115.60 (s), 108.66 (s), 77.26 (s), 77.05 (s), 76.84 (s), 68.23 (s), 42.96 (s), 29.11 (s), 28.85 (s), 23.94 (s). HRMS (ESI) peaks of m/z value for was calculated 596.1830 and observed 596.1842. (**Figure-S19-S21**).

2,2'-(5-((6-(9H-carbazol-9-yl)hexyl)oxy)-1,3-phenylene)bis(benzothiazole) [BT2O6Cz]: ^{1}H NMR (600 MHz, $CDCl_3$) δ 8.33 (s, 1H), 8.11 (t, *J* = 7.5 Hz, 4H), 7.94 (d, *J* = 7.8 Hz, 2H), 7.76 (s, 2H), 7.53 (t, *J* = 7.6 Hz, 2H), 7.47 (dd, *J* = 16.9, 9.8 Hz, 4H), 7.42 (d, *J* = 8.0 Hz, 2H), 7.23 (t, *J* = 7.3 Hz, 2H), 4.36 (t, *J* = 7.2 Hz, 2H), 4.14 (t, *J* = 6.3 Hz, 2H), 1.98 – 1.94 (m, 2H), 1.86 – 1.82 (m, 2H), 1.59 – 1.56 (m, 2H), 1.52 – 1.48 (m, 2H). ^{13}C NMR (151 MHz, $CDCl_3$) δ 166.99 (s), 159.96 (s), 154.02 (s), 140.42 (s), 135.64 (s), 135.22 (s), 126.51 (s), 125.59 (d, *J* = 18.1 Hz), 123.43 (s), 122.84 (s), 121.75 (s), 120.39 (s), 119.17 (s), 118.77 (s), 115.62 (s), 108.66 (s), 77.26 (s), 77.05 (s), 76.84 (s), 68.36 (s), 42.98 (s), 29.13 (s), 28.99 (s), 27.10 (s), 25.96 (s). HRMS (ESI) peaks of m/z was calculated 610.1987 and observed 610.1993. (**Figure-S22-S24**).

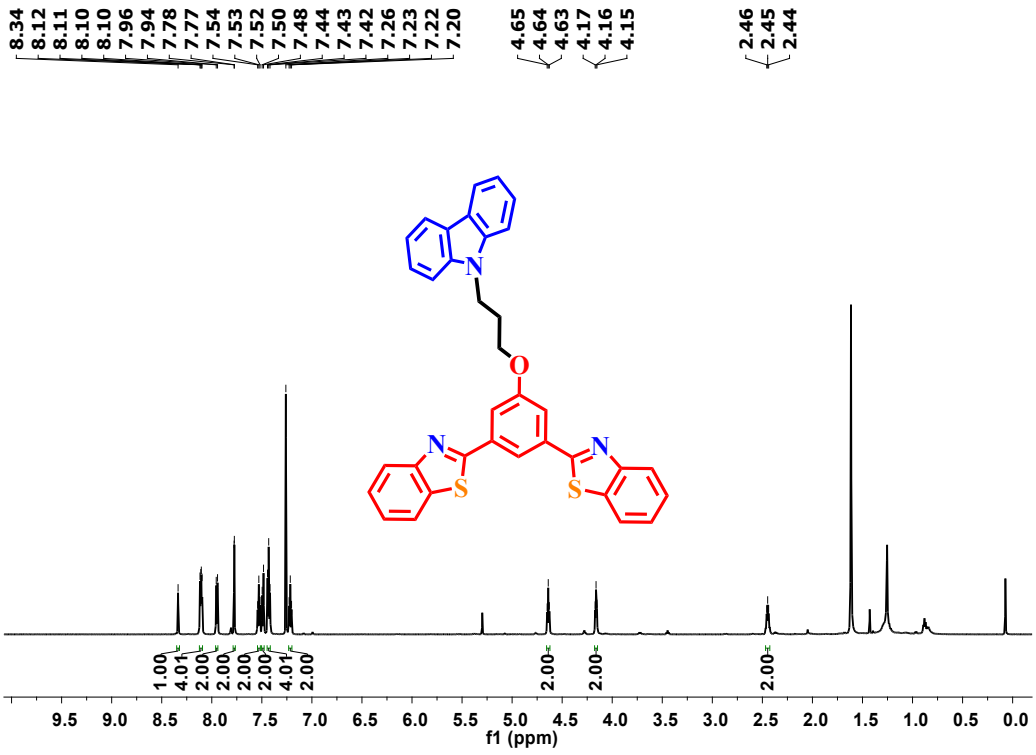

Figure S14. ^{1}H NMR spectra of BT2O3Cz in $CDCl_3$ at 298K.

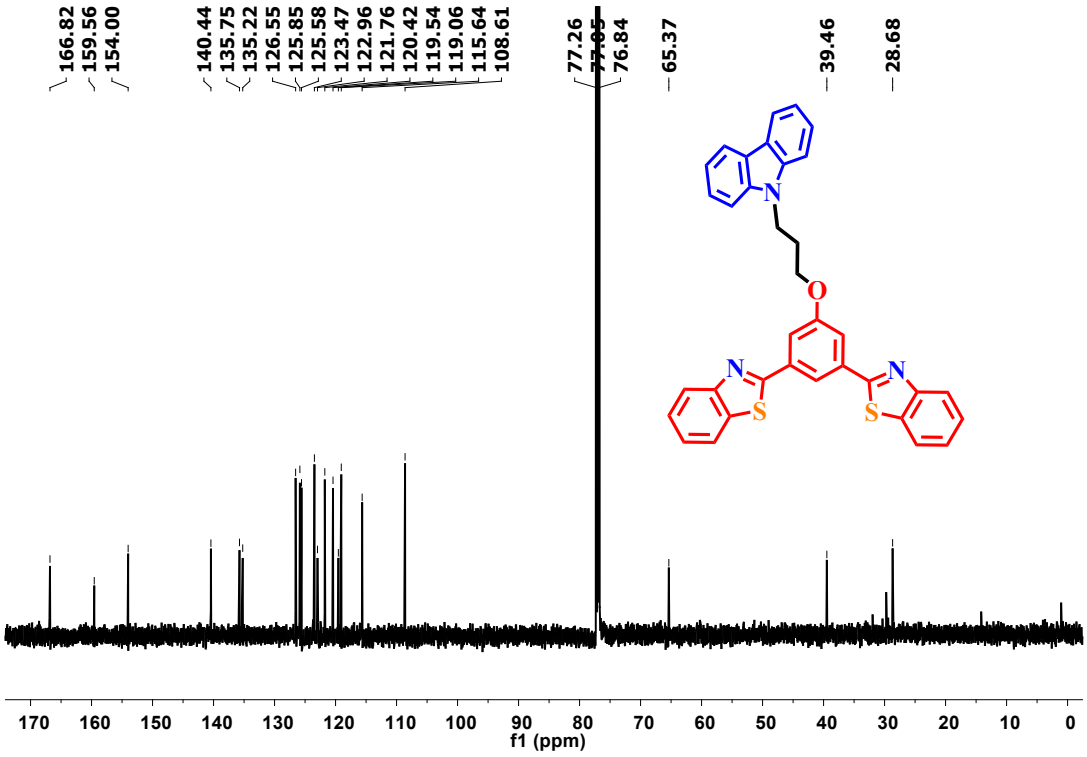

Figure S15. ^{13}C- NMR spectra of BT2O3Cz in $CDCl_3$ solvent at 298 K.

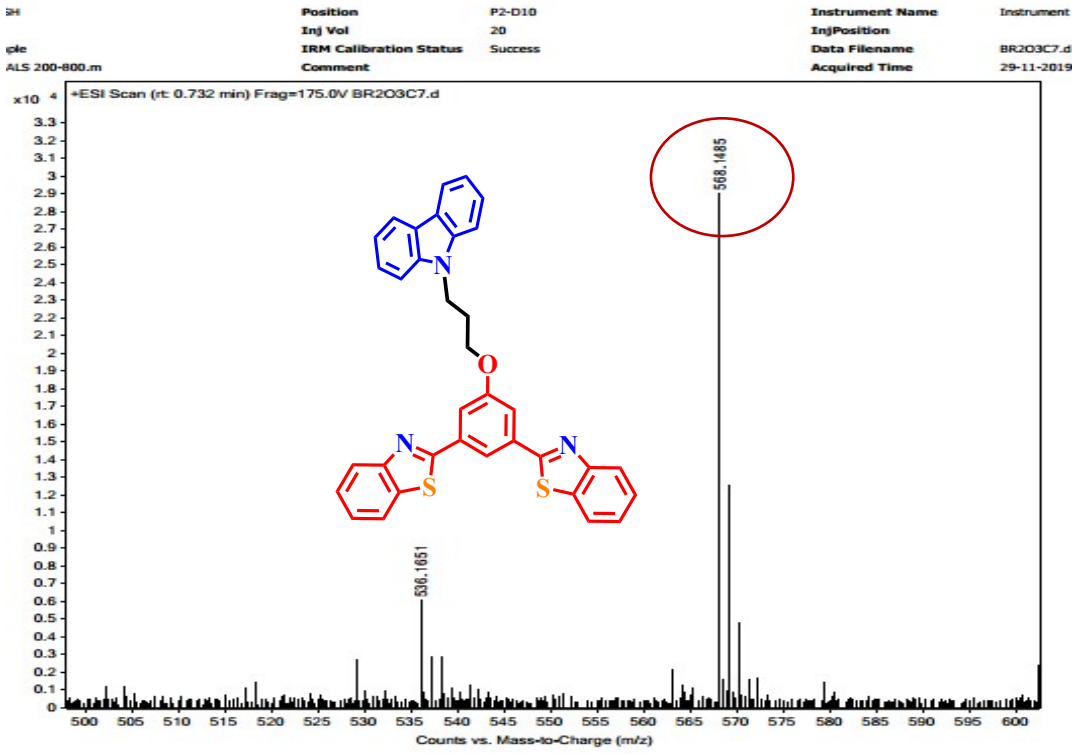

Figure S16. HRMS (ESI) peaks of m/z value for $[BT2O3Cz + H]^+$ was calculated 568.1517 and observed 568.1485 at 298K in Acetonitrile solvent.

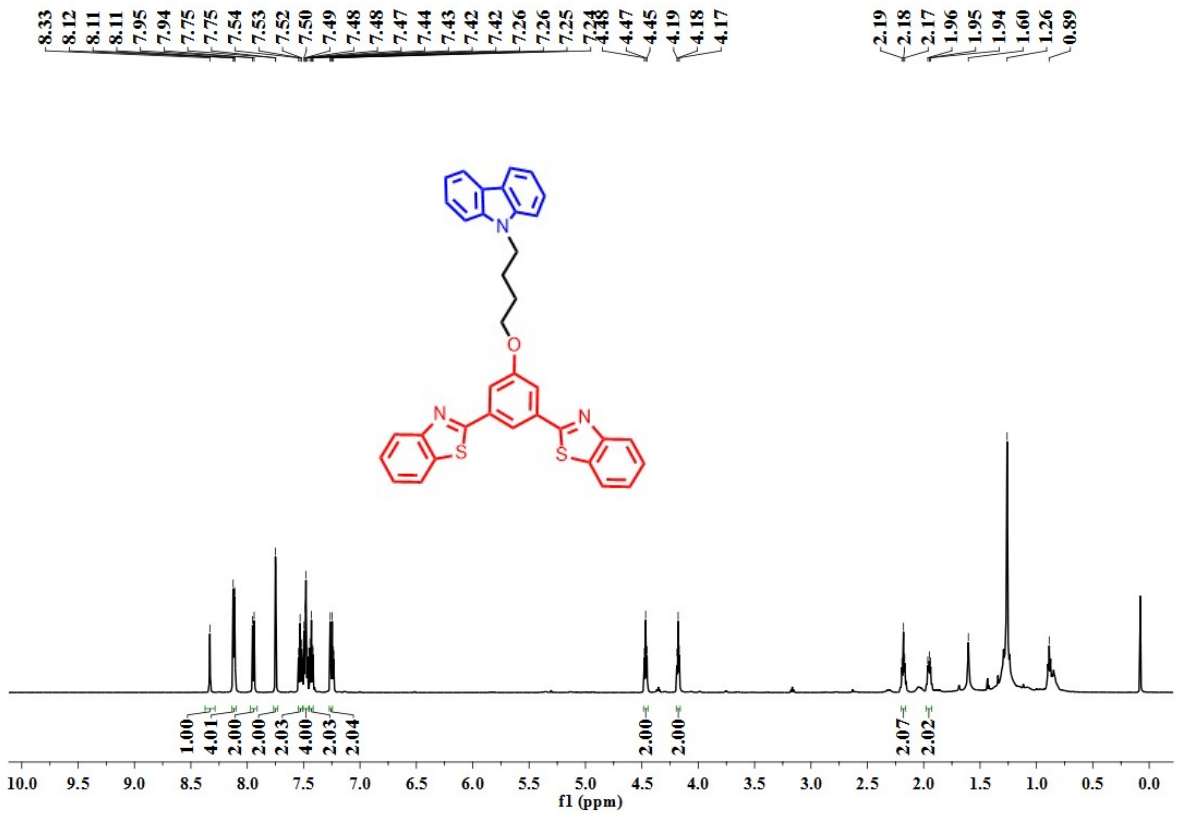

Figure S17. ^{1}H NMR spectra of BT2O4Cz in $CDCl_3$ at 298K.

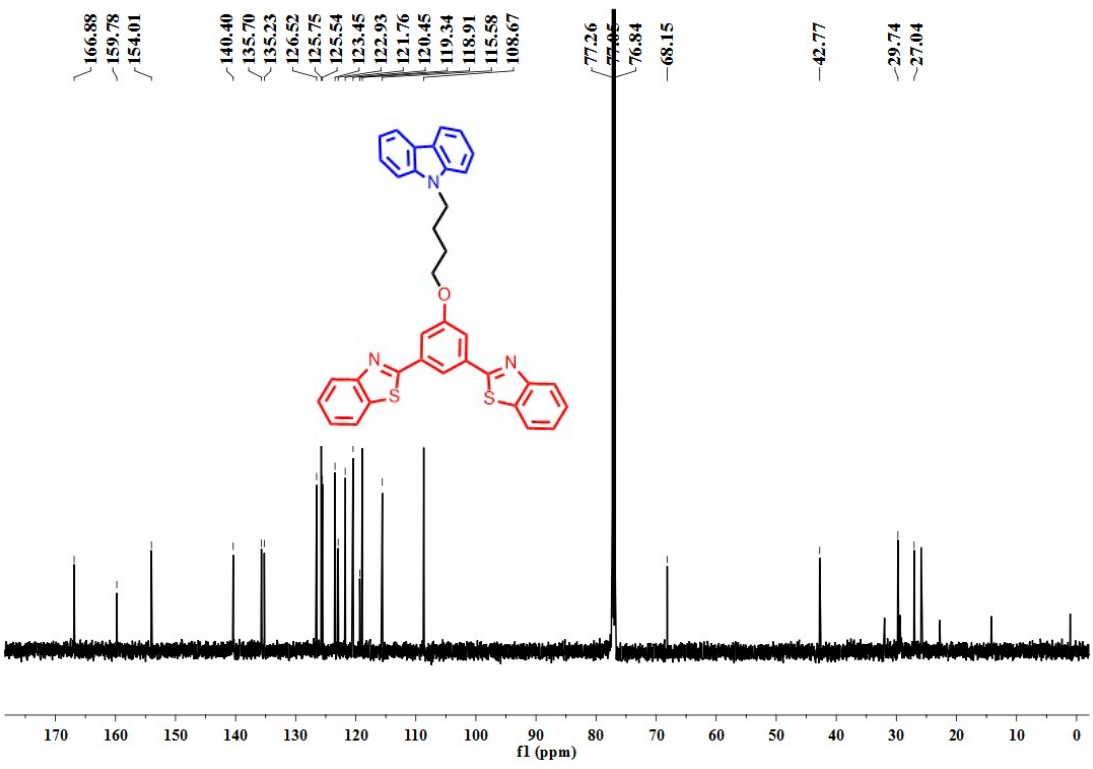

Figure S18. ^{13}C- NMR spectra of BT2O4Cz in $CDCl_3$ solvent at 298 K.

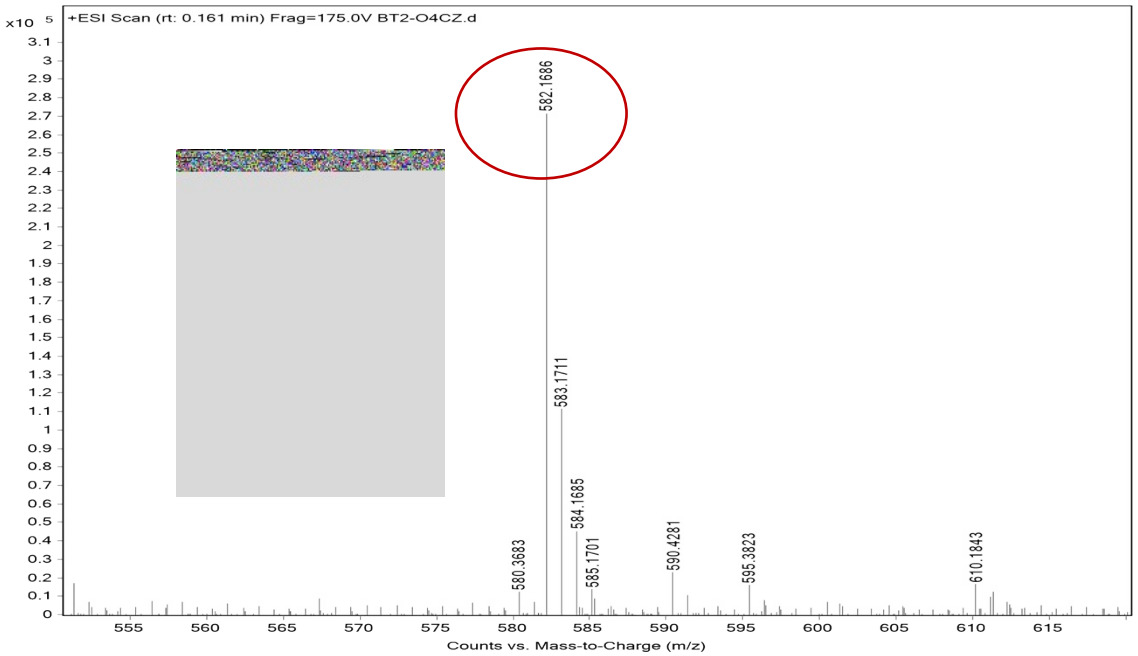

Figure S19. HRMS (ESI) peaks of m/z value for $[BT2O4Cz + H]^+$ was calculated 582.1674 and observed 582.1686 at 298K in HPLC Acetonitrile solvent.

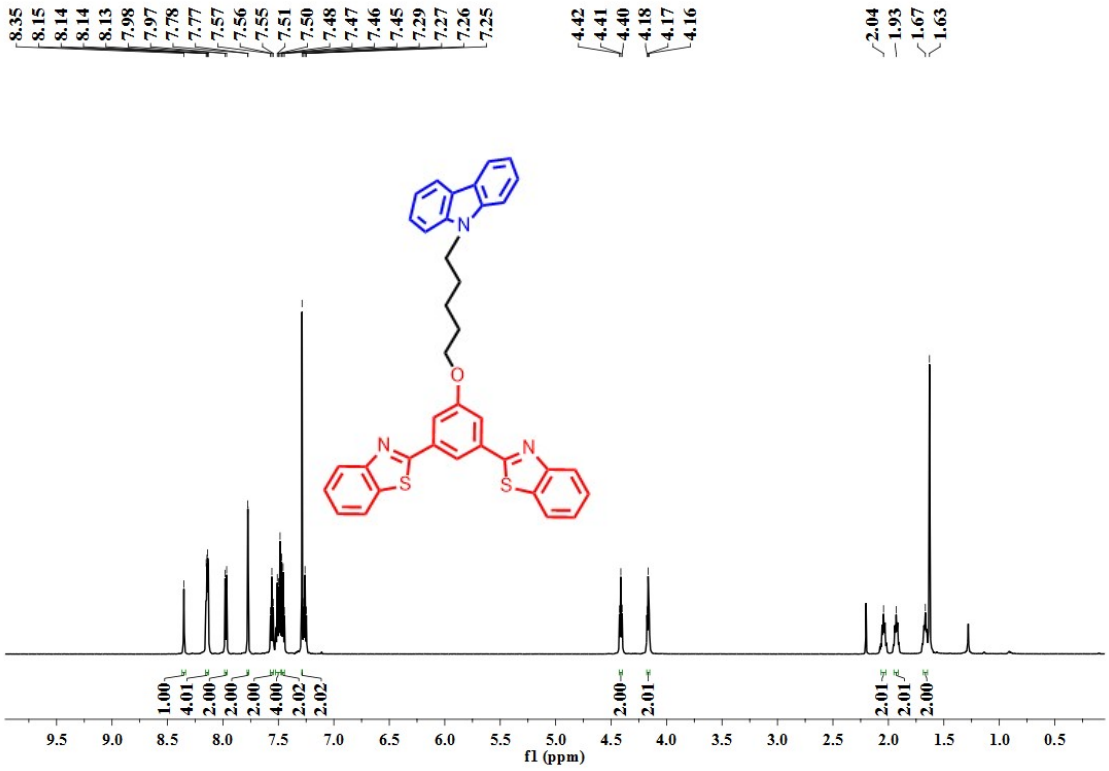

Figure S20. ^1H NMR spectra of BT2O5Cz in $CDCl_3$ at 298K.

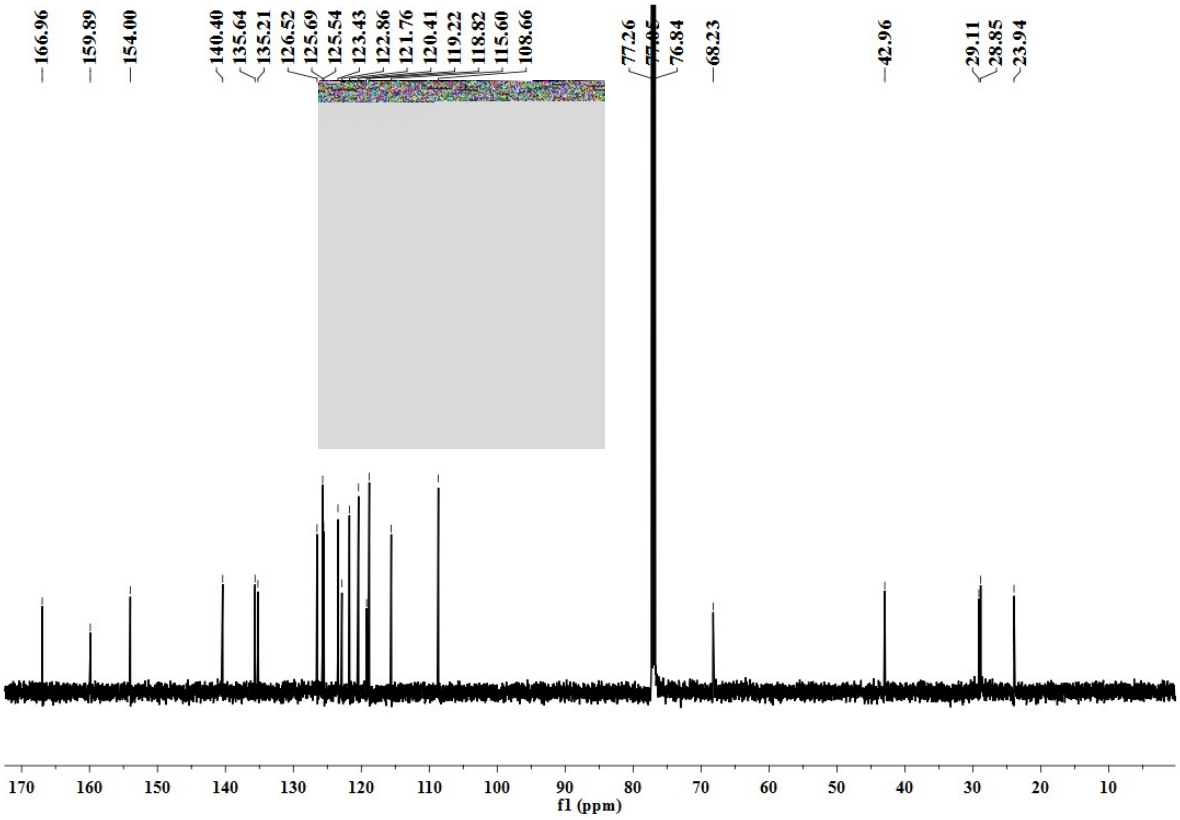

Figure S21. ^{13}C- NMR spectra of BT2O5Cz in $CDCl_3$ solvent at 298 K.

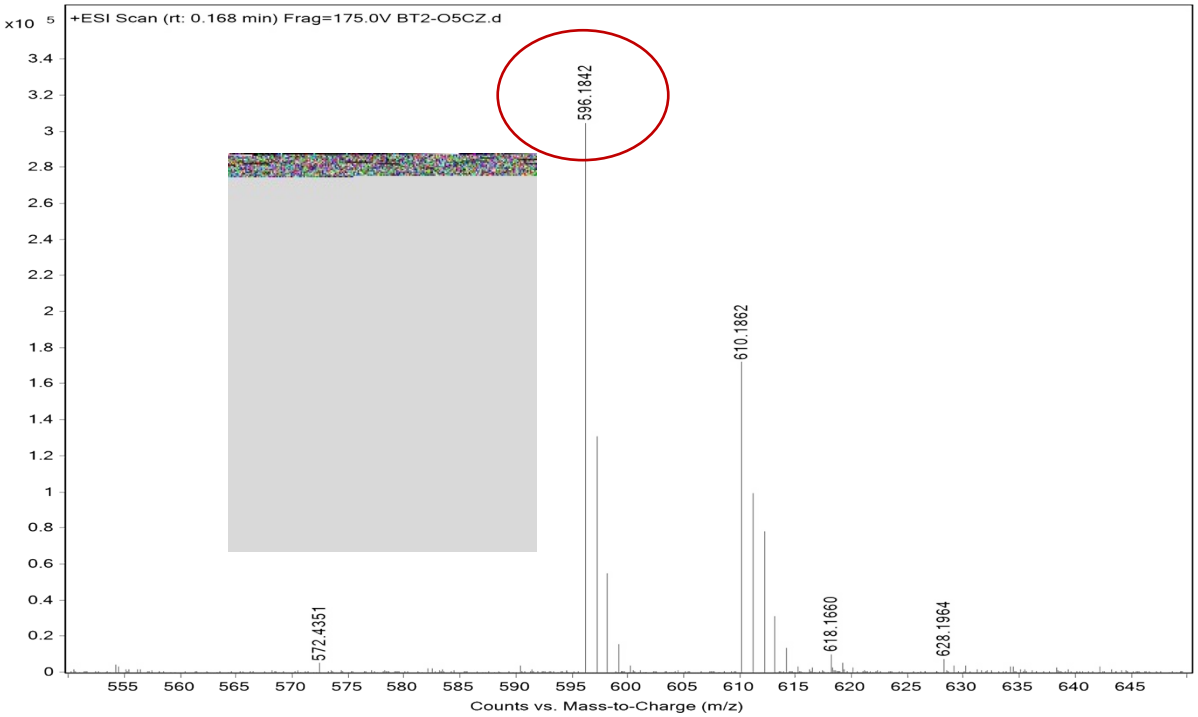

Figure S22. HRMS (ESI) peaks of m/z value for $[BT2O5Cz + H]^+$ was calculated 596.1830 and observed 596.1842 at 298K in HPLC Acetonitrile solvent.

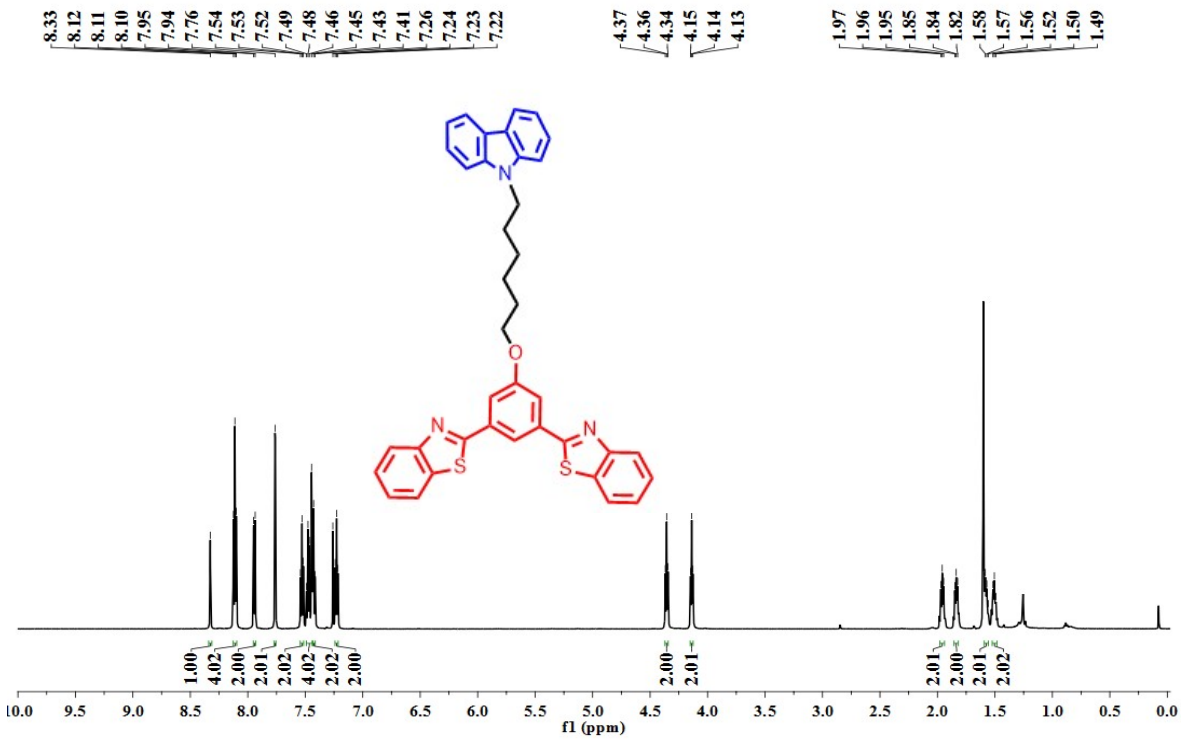

Figure S23. ^{1}H NMR spectra of BT2O6Cz in $CDCl_3$ at 298K.

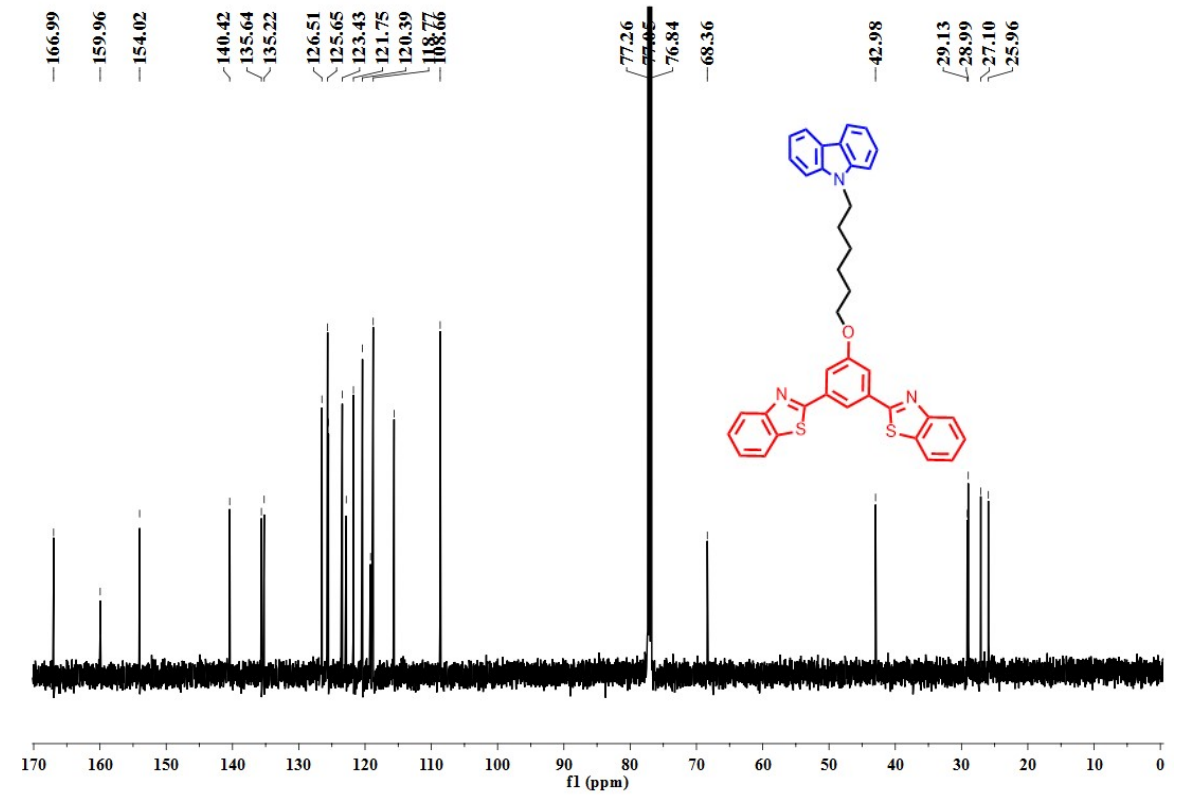

Figure- S24. ^{13}C- NMR spectra of BT2O6Cz in $CDCl_3$ solvent at 298 K.

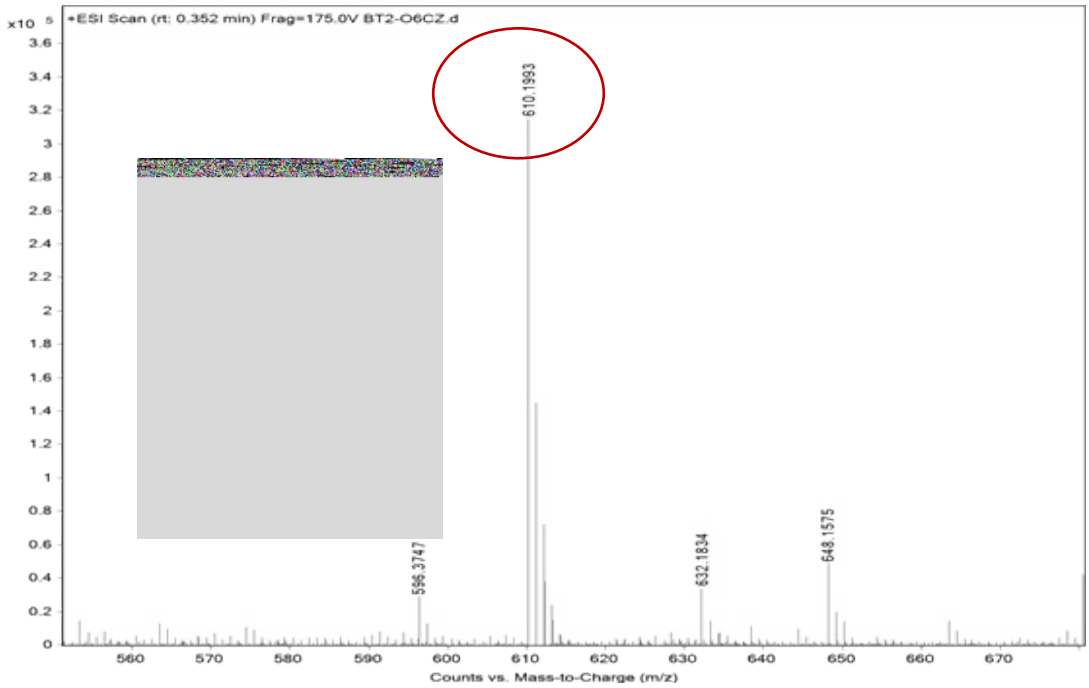

Figure S25. HRMS (ESI) peaks of m/z value for $[BT2O6Cz + H]^+$ was calculated 610.1987 and observed 610.1993 at 298K in HPLC Acetonitrile solvent.

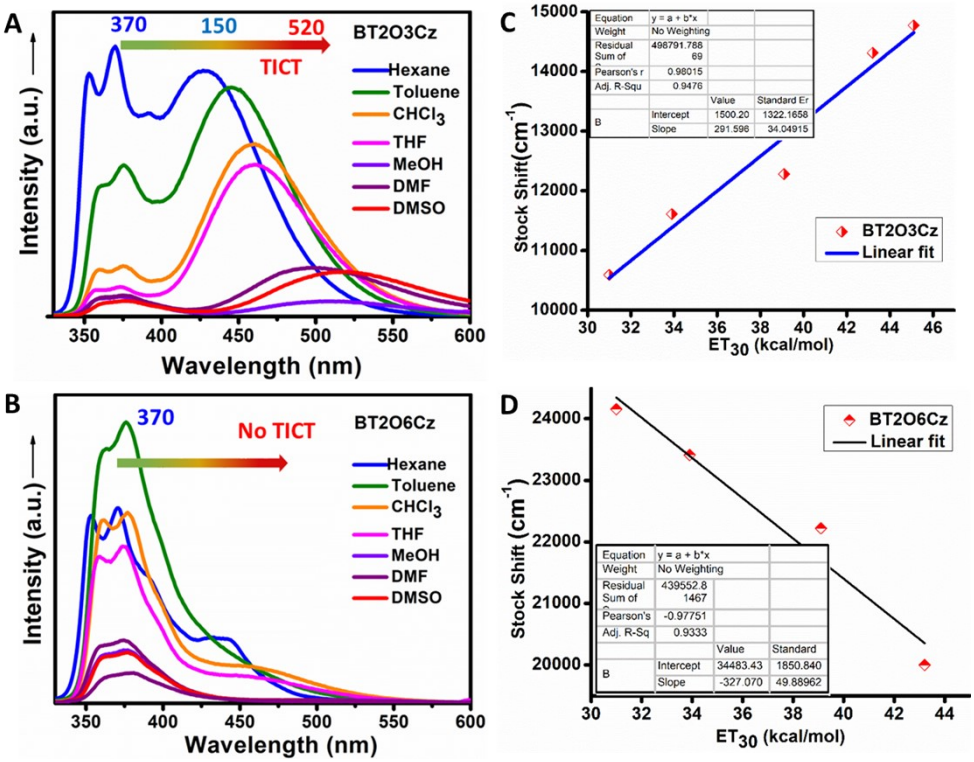

Figure S26. Solvatochromism study: (A, B) Fluorescence spectra of BT2O3Cz and BT2O6Cz (1 x 10^{-5} M)) at various solvent with varying polarity, to understand the through-space twisted intramolecular charge transfer (TSTICT) behavior on varying the alkyl chain length between donor and acceptor. (C, D) The extent of solvatochromism was tested by the

Lippert-Mataga plot Stokes shift of BT2O5Cz in different solvents, plotted against their ET(30) values and fitted with straight line (using equation S2). Notably, the Stokes shift and emission maxima of BT2O3Cz and BT2O6Cz showed positive and negative slope with the increase of solvent polarity.

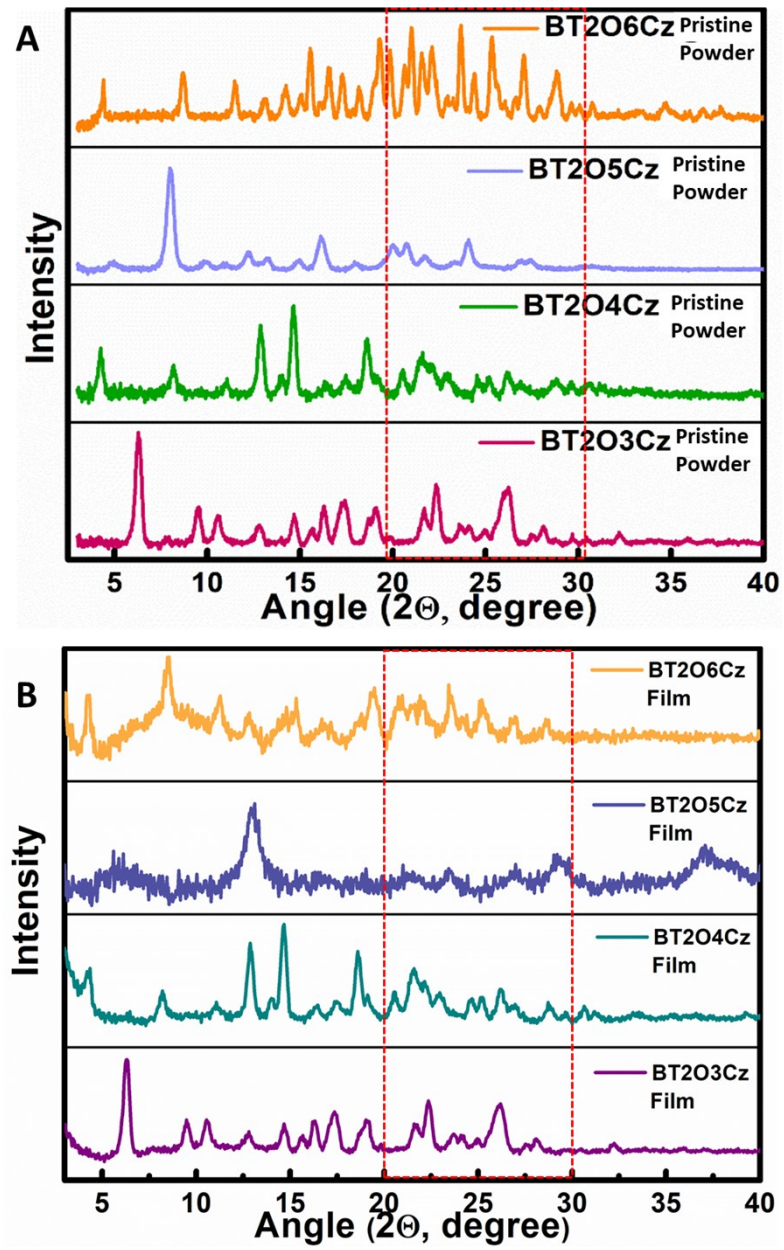

Figure S27. PXRD (A) and thin film XRD (B) for all the emitters, BT2OxCz (x=3,4,5,6) at their pristine powder form and drop-casted thin film state. In both XRD patterns, the broad peaks observed for BT2O5Cz, whereas, other emitters of BT2OxCz (x =3,4,6) showed sharp diffracting peak patterns at low d-spacing region (marked in red dotted box) depicting high degree of crystallinity of BT2OxCz (n =3,4,6) and amorphous nature of BT2O5Cz.

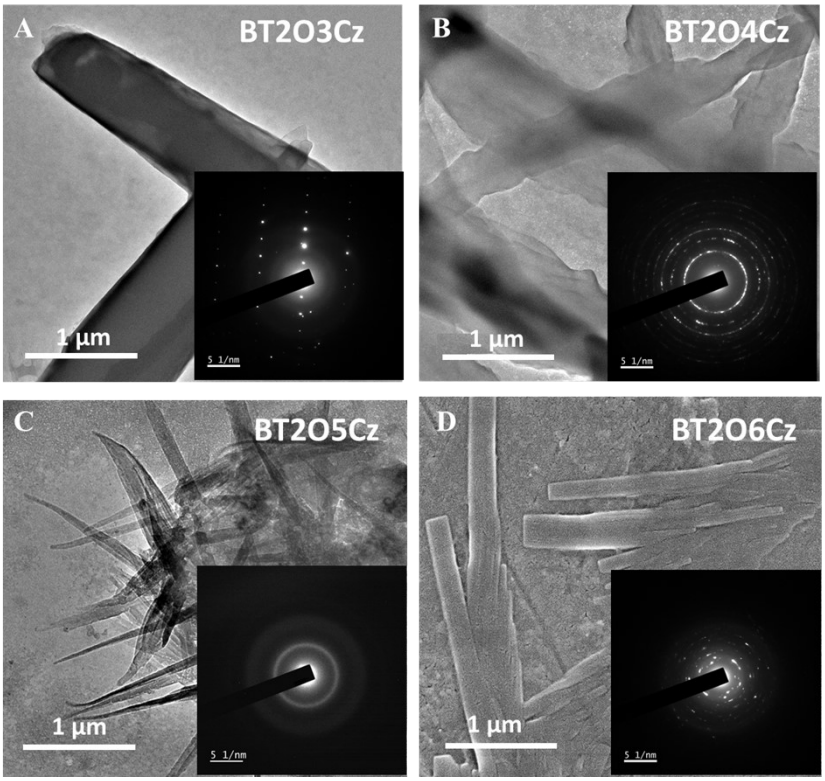

Figure S28. FETEM images (inset: SAED images) of BT2OxCz (x=3, 4, 5 & 6). Samples were prepared from THF solution and by drop casting technique on copper grid (400 mesh). All the emitters exhibited nearly similar micro-rod shaped morphology. However, SAED images showed amorphous nature of BT2O5Cz, while all other emitters are found to be crystalline in nature.

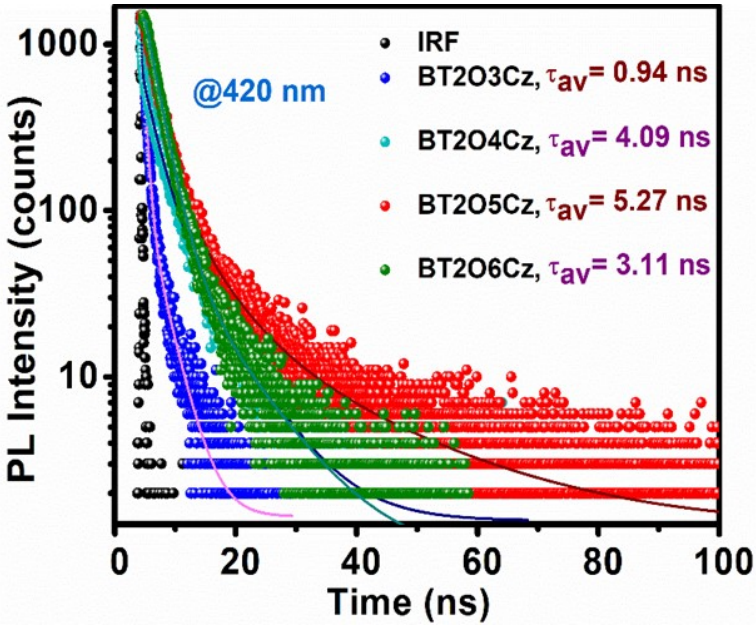

Figure S29. Prompt fluorescence/LE state emission lifetime recorded in crystalline powder form for all the emitters, BT2OxCz (x=3,4,5,6) at 420 nm.

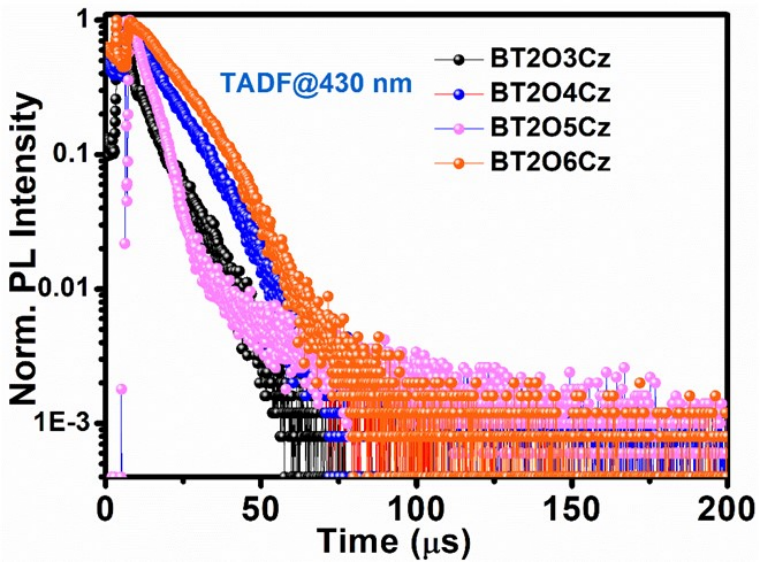

Figure S30. Delayed fluorescence lifetime recorded in crystalline powder form for all the emitters, BT2OxCz (x=3,4,5,6) at 430 nm.

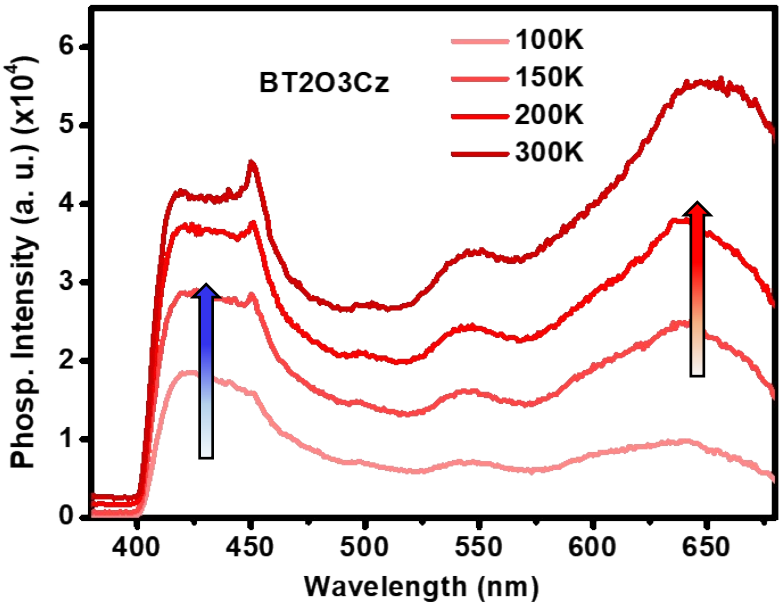

Figure S31. Temperature dependent delayed emission recorded in crystalline powder form for BT2O3Cz.

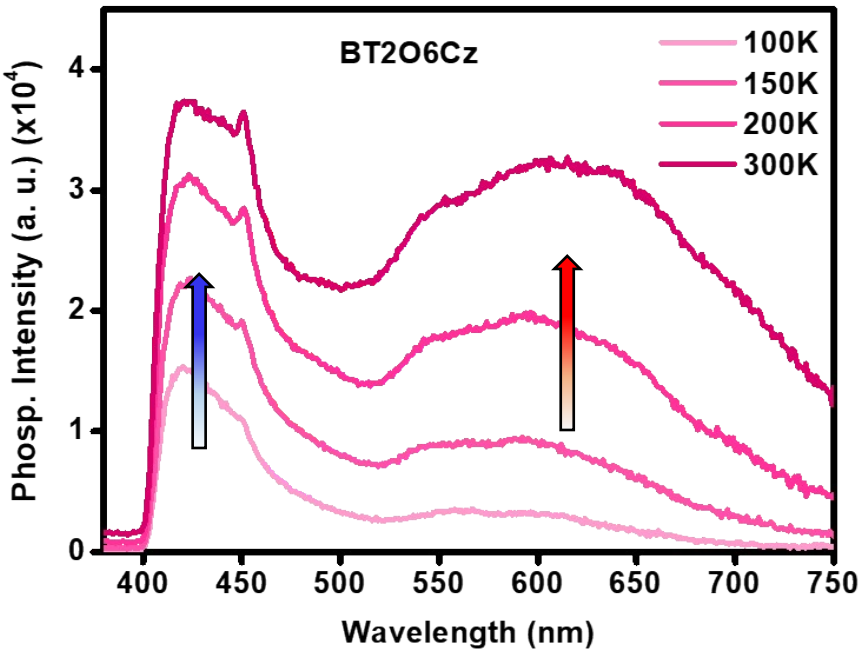

Figure S32. Temperature dependent delayed emission recorded in crystalline powder form for for BT2O6Cz.

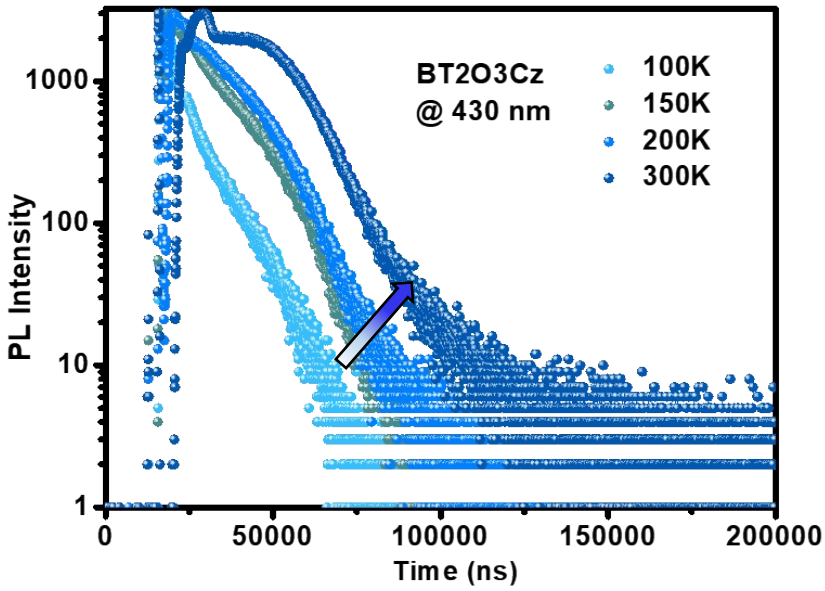

Figure S33. Temperature dependent delayed emission decay recorded in crystalline powder form for for BT2O3Cz for at 430 nm.

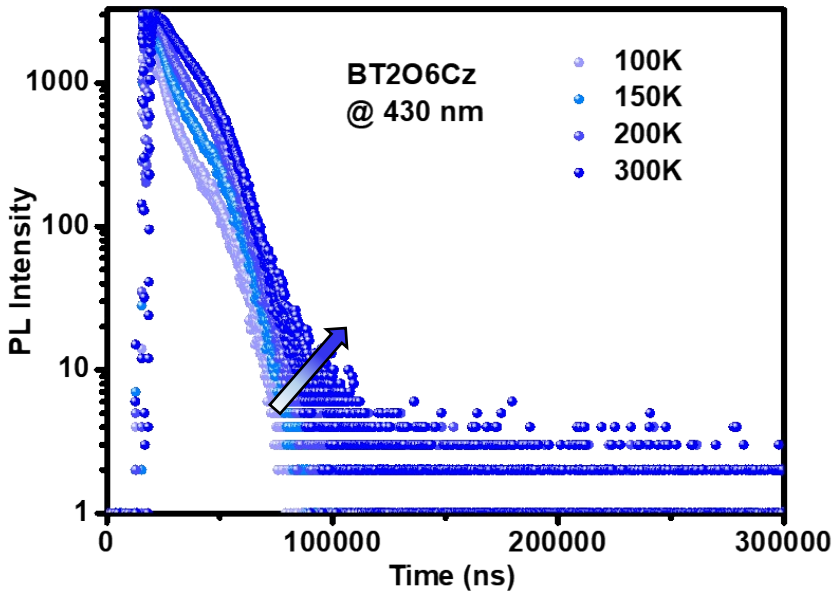

Figure S34. Temperature dependent delayed emission decay recorded in crystalline powder form for BT2O6Cz for at 430 nm.

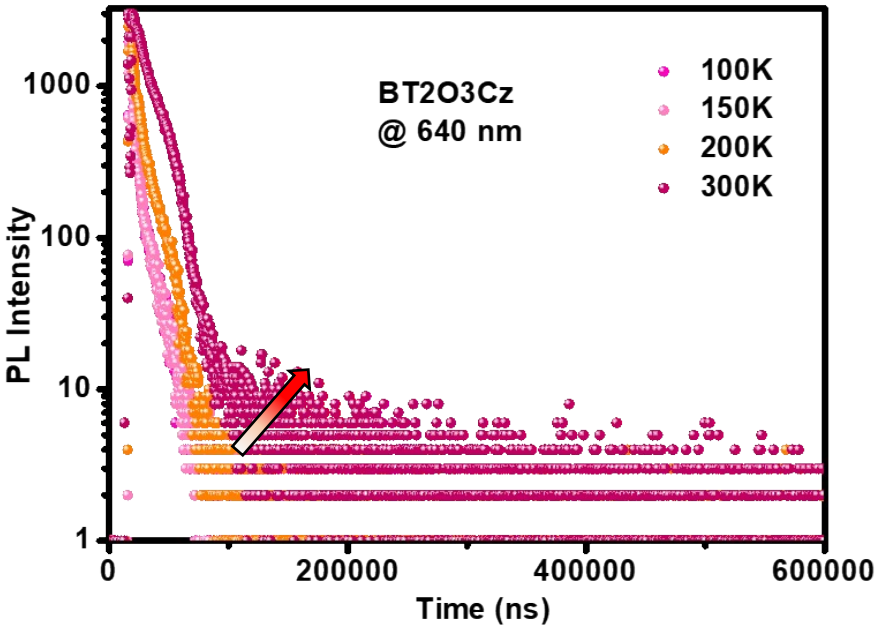

Figure S35. Temperature dependent phosphorescence emission recorded in crystalline powder form for for BT2O3Cz at 640 nm.

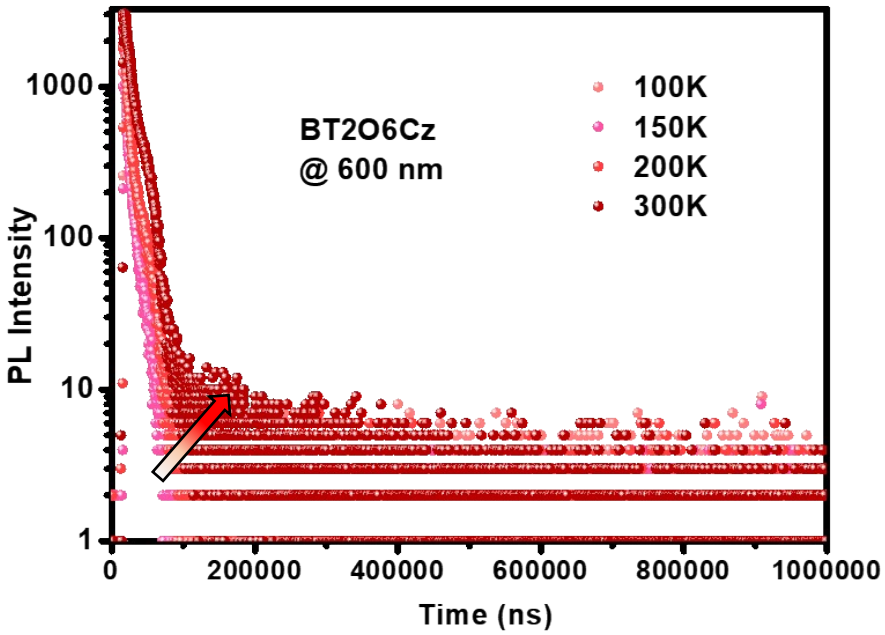

Figure S36. Temperature dependent phosphorescence decay recorded in crystalline powder form for BT2O6Cz for at 600 nm.

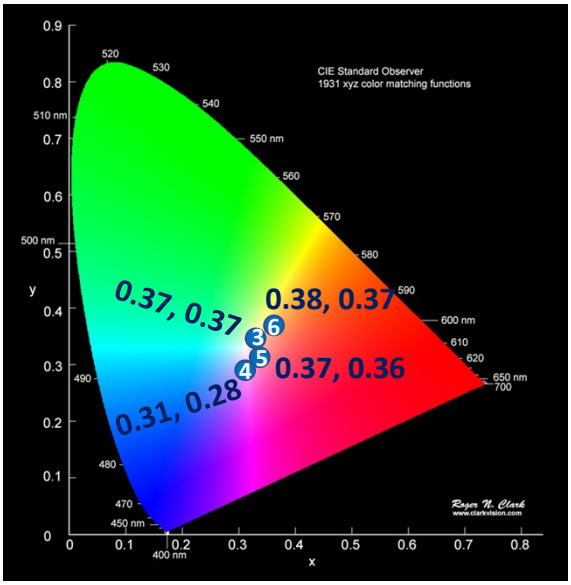

Figure S37. CIE diagram plotted for 0.5 % PMMA doped spin coated film for BT2OxCz (x=3,4,5,6).

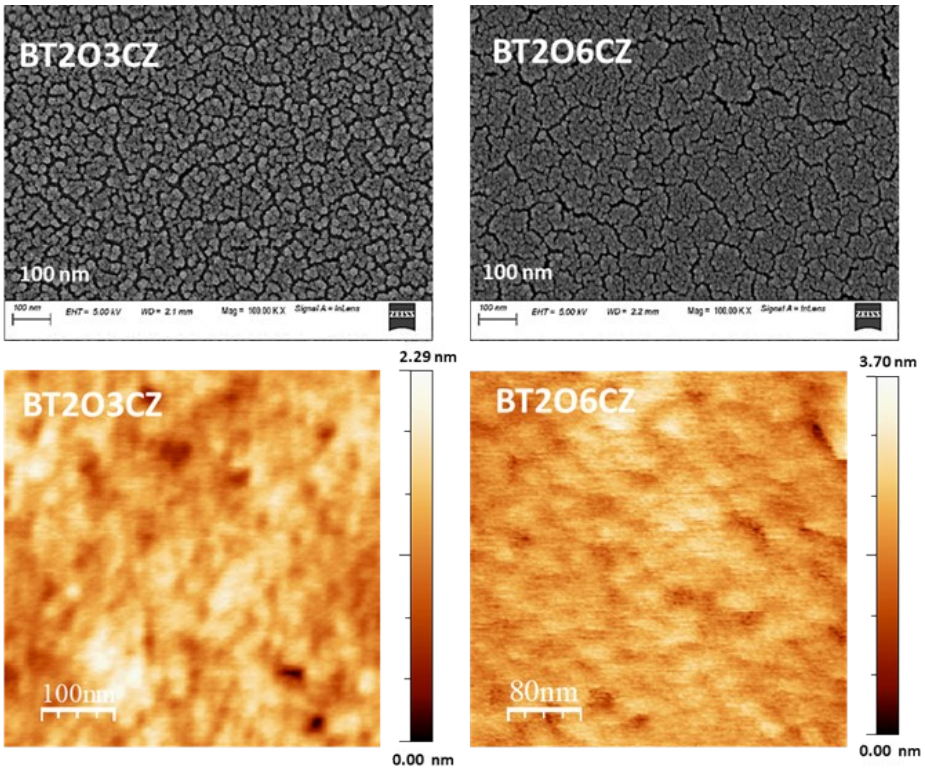

Figure S38. AFM images recorded for 0.5 % PMMA doped spin coated film for BT2O3Cz and for BT2O6Cz respectively.

Table S1. Summary of Excited state kinetics for solid powder form of all the OSMWLEs.

Emitters	k_P ($x10^7$ s^{-1})	k_D ($x10^5$ s^{-1})	k_F ($x10^7$ s^{-1})	k_{IC} ($x10^7$ s^{-1})	k_{ISC} ($x10^6$ s^{-1})	k_{RISC} ($x10^5$ s^{-1})
BT2O3Cz	106	1.47	25.5	80.4	7.5	1.47
BT2O4Cz	24.4	0.91	4.8	3.8	1.53	0.24
BT2O5Cz	18.9	0.46	3.0	15.7	1.25	0.46
BT2O6Cz	32.1	0.48	5.4	26.3	0.75	0.48

All the excited kinetics values calculated from Equation S3-S8.

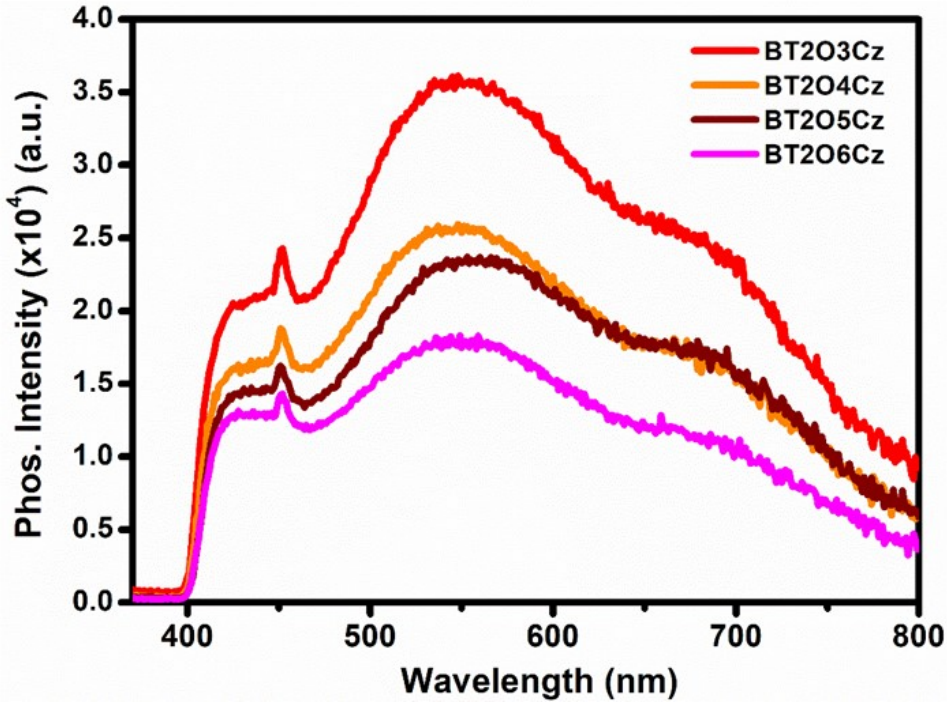

Figure S39. Phosphorescence spectra recorded for 5.0 % PMMA doped spin coated film for BT2O3Cz and for BT2O6Cz respectively.

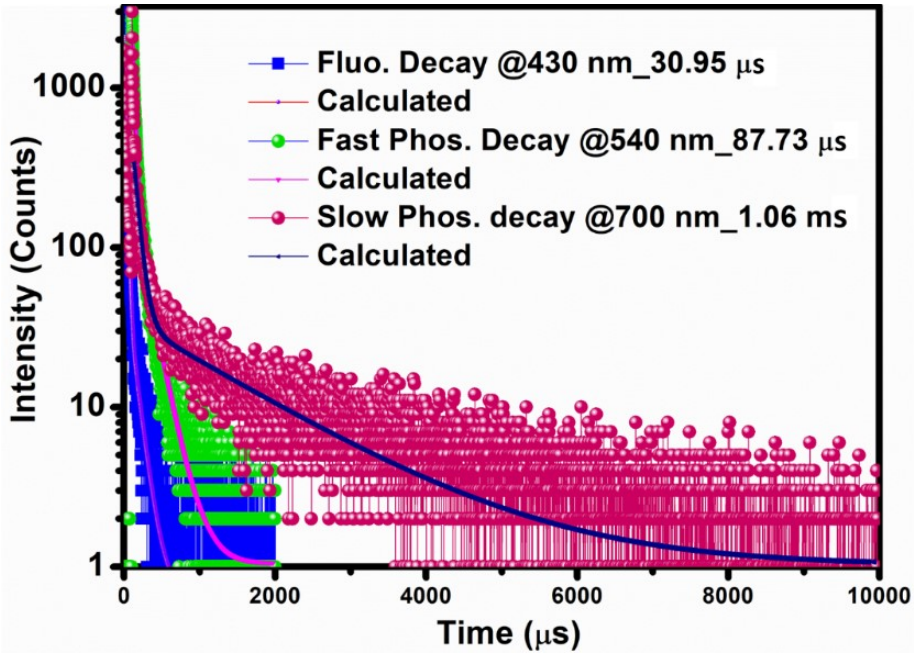

Figure S40. Phosphorescence decay recorded for 5.0 % PMMA doped spin coated film for BT2O3Cz for the respective emission band centered at 430, 540 and 700 nm respectively.

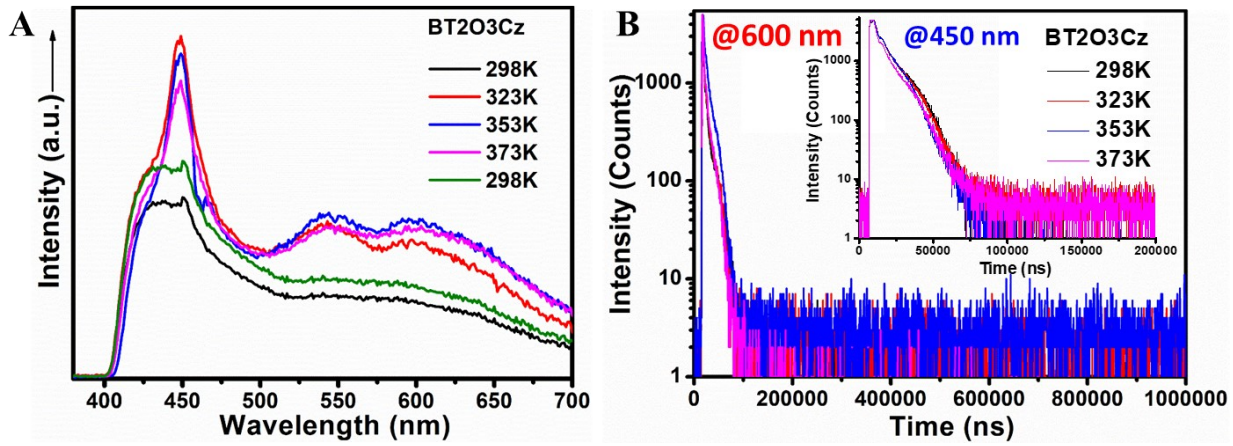

Figure S41. Phosphorescence decay recorded at different temperatures for white film for BT2O3Cz for the respective TADF and phosphorescence band centered at 450 and 600 nm respectively.

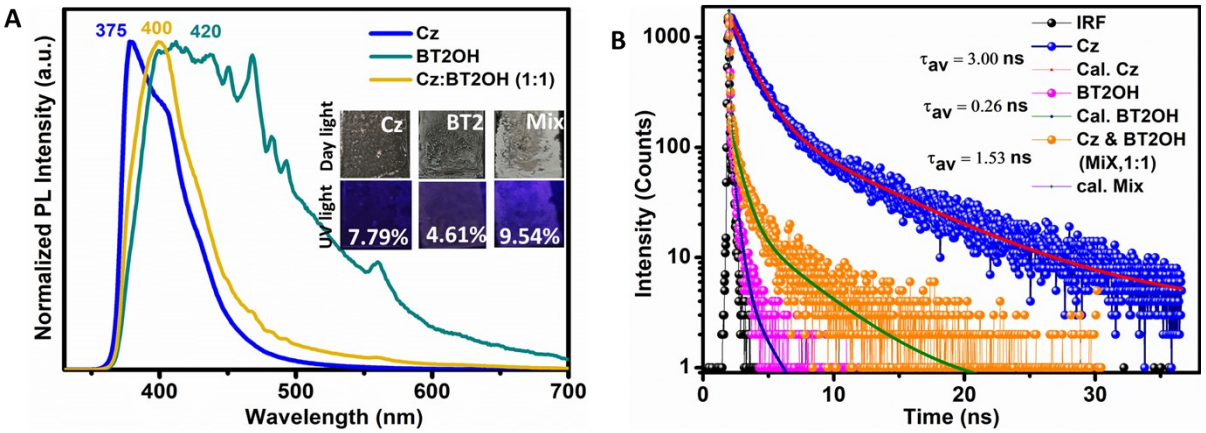

Figure S42. Film PL spectra and TRPL of each moiety (Cz, BT2OH) and mixture (Cz:BT2OH = 1:1) (A & B). Locally excited state emission due to the π-π* transitions including triexponential decay fit of BT2OH and mixture, while the Cz showed biexponential fit revealing prompt and delayed species present in the system.

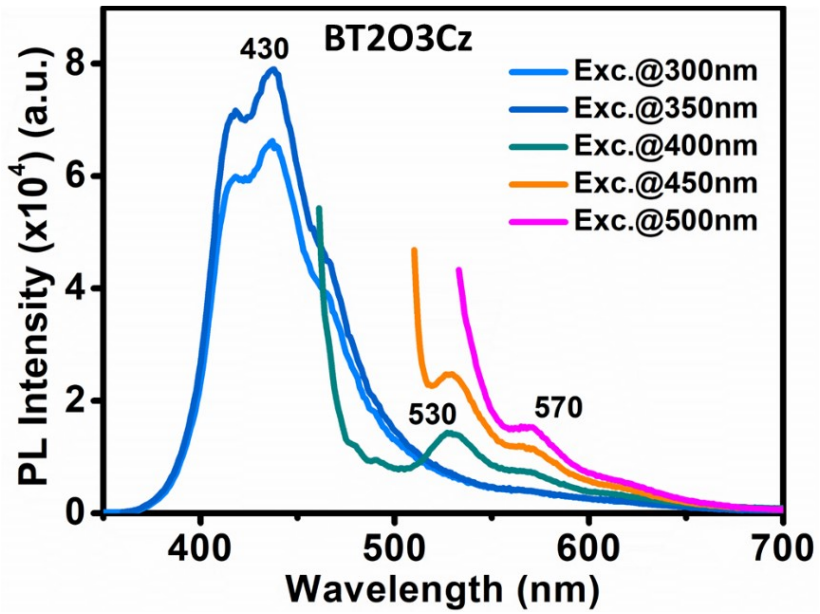

Figure S43. Excitation-dependent corrected emission spectra of compound BT2O3Cz. The bright state fluorescent spectra that were obtained after exciting at λ_{ex} = 320 nm, where dark state spectra were obtained by exciting λ_{ex} = 500 nm and amplified by two times for the sake of clarity.

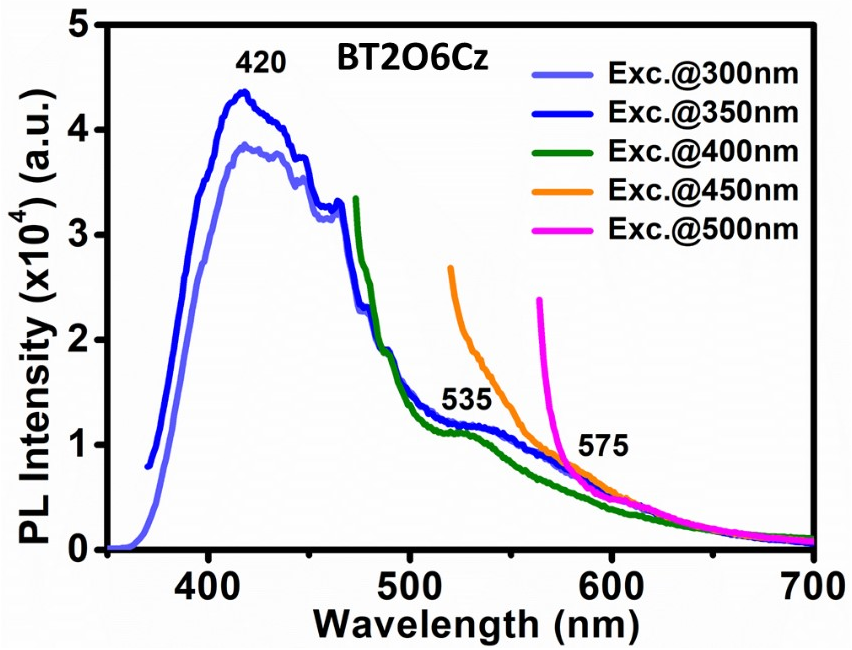

Figure S44. Excitation-dependent corrected emission spectra of compound BT2O6Cz. The bright state fluorescent spectra that were obtained after exciting at λ_{ex} = 320 nm, where dark state spectra were obtained by exciting λ_{ex} = 500 nm and amplified by two times for the sake of clarity.

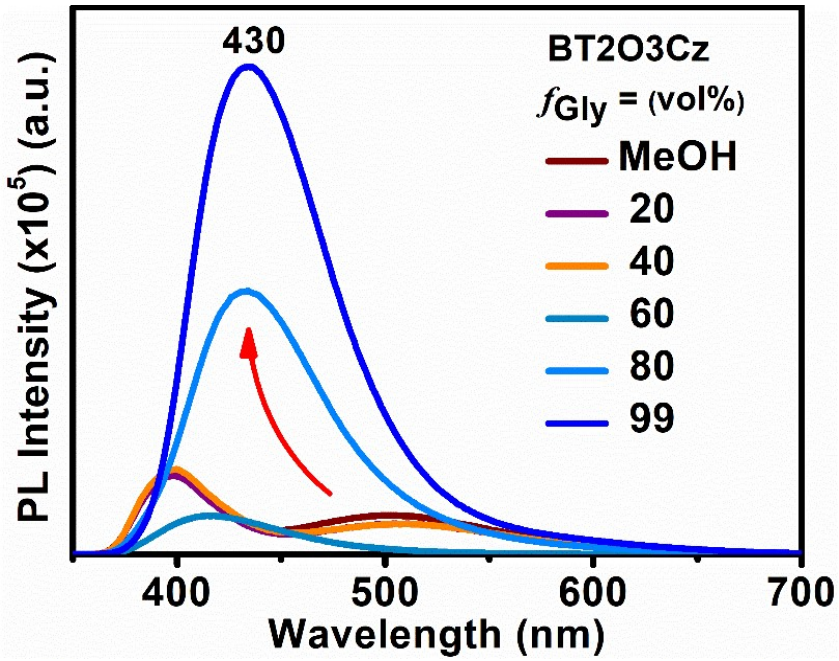

Figure S45. Fluorescence spectra of compound BT2O3Cz in mixtures of glycerol and methanol of increased solvent viscosity and results in an almost fifteen fold increase in emission intensity.

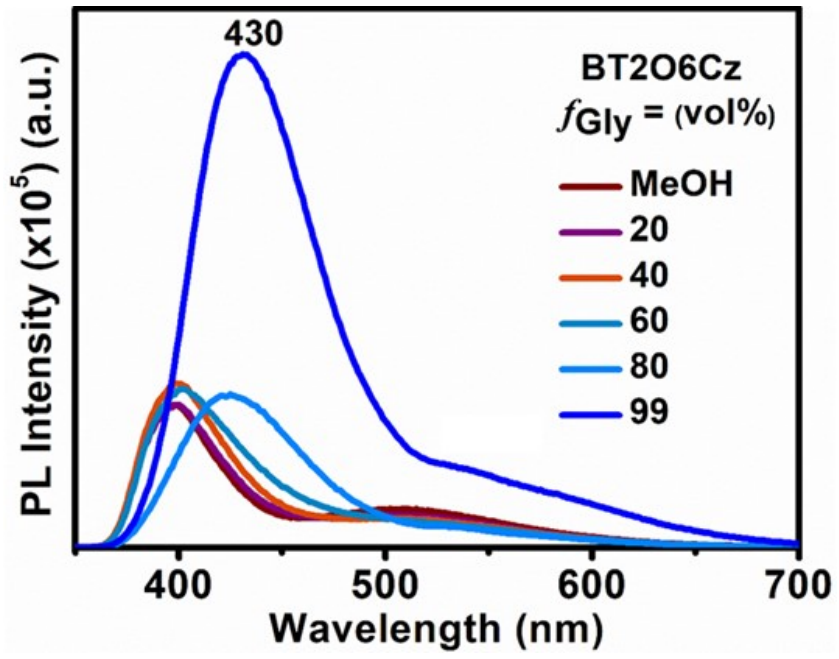

Figure S46. Fluorescence spectra of compound BT2O6Cz in mixtures of glycerol and methanol of increased solvent viscosity and results in an almost fifteen fold increase in emission intensity.

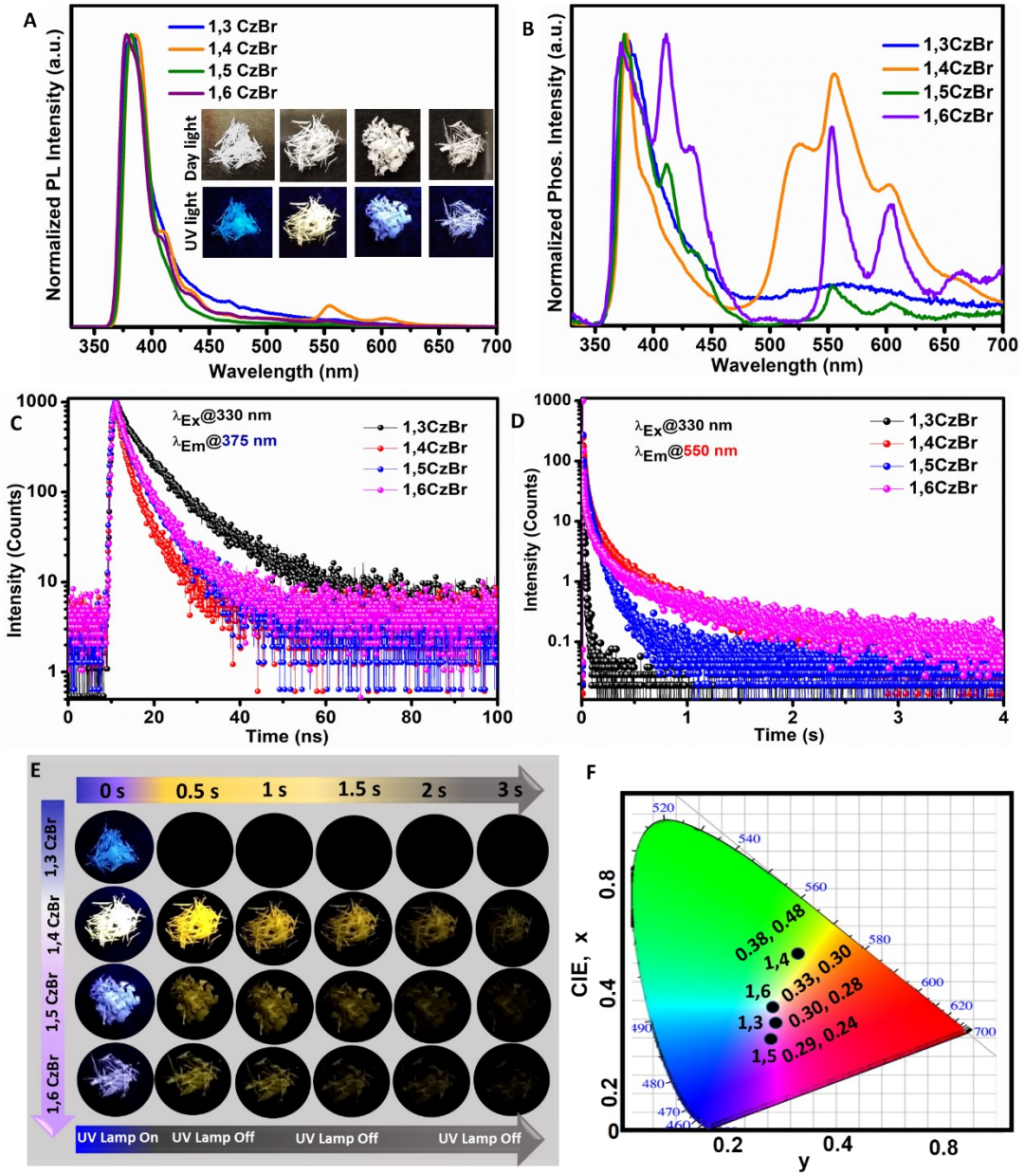

Figure S47. Ultra-long room temperature phosphorescence (URTP) study for various alkyl chain containing carbazole unit, 1,n CzBr (n =3, 4, 5, & 6). (A) Steady state PL spectra exhibited a sharp band near 375 nm due to delayed fluorescence and shoulder peaks near 550 nm, due to phosphorescence. (B) Phosphorescence spectra were recorded in air and found to be very distinct phosphorescence centered at ~ 550 nm. (C & D) Prompt fluorescence decay (ns) and phosphorescence decay (ms) was recorded in air for 375 and 550 nm respectively. (E) URTP emissions were further captured under UV-light (365 nm) at both on and off conditions. (F) CIE-coordinates values revealed the white phosphorescence emission for 1,6 CzBr.

Fast phosphorescence emission at 550 nm observed from the present BT2OxCz emitter is inherited from the bromo-alkylated carbazole derivatives which is due to the impurity effect. The hypothesis was further confirmed by high-performance liquid chromatograohy (HPLC) (Figure S40-41) study.

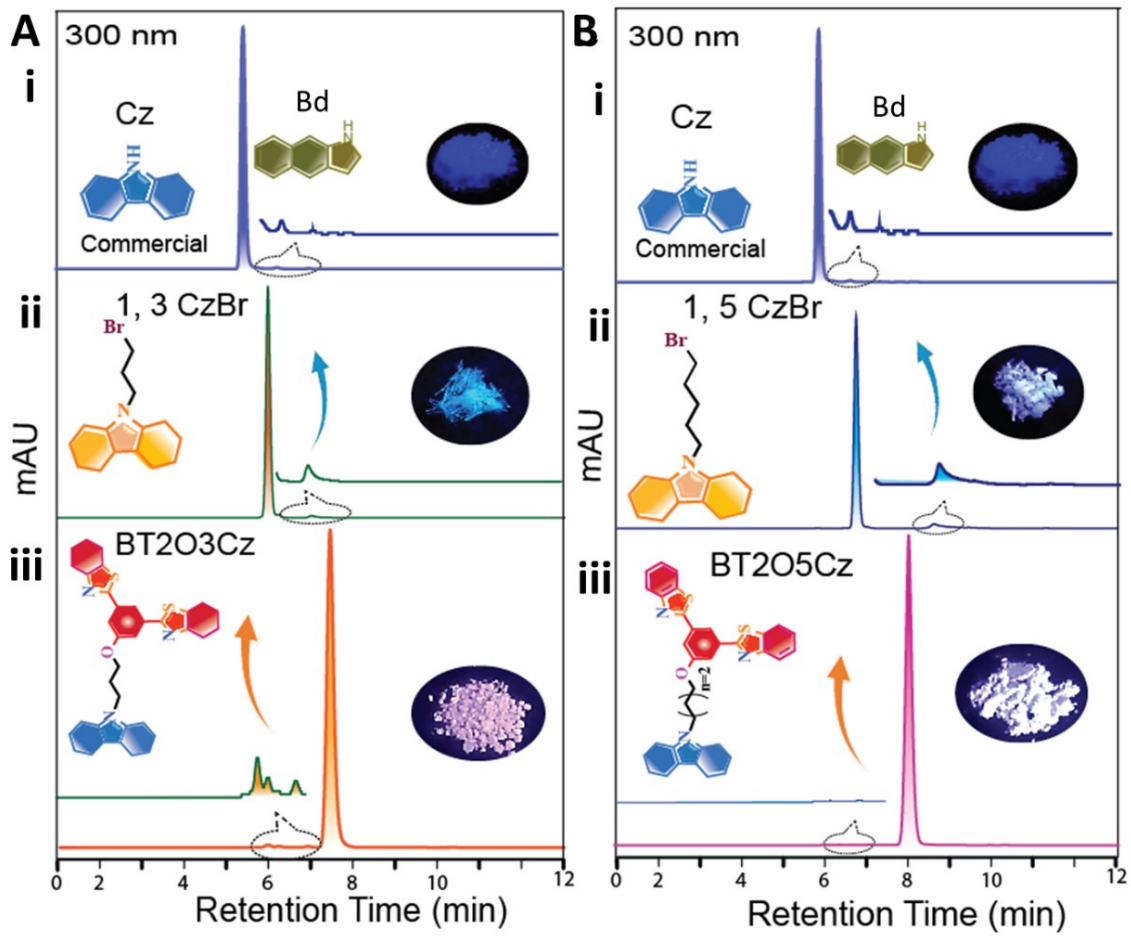

Figure S48. (A, B) HPLC spectra of commercial Cz (i), 1,3CzBr, 1,5CzBr crystals(ii) and BT2O3Cz, BT2O5Cz crystals (iii) monitored at 300nm with acetonitrile as eluent. For all the crystals up to final compounds inherits an impurity peak of Bd compounds. Chemical structure of all the compounds were shown with inset photograph of each crystal captured under 365 nm UV-lamp.

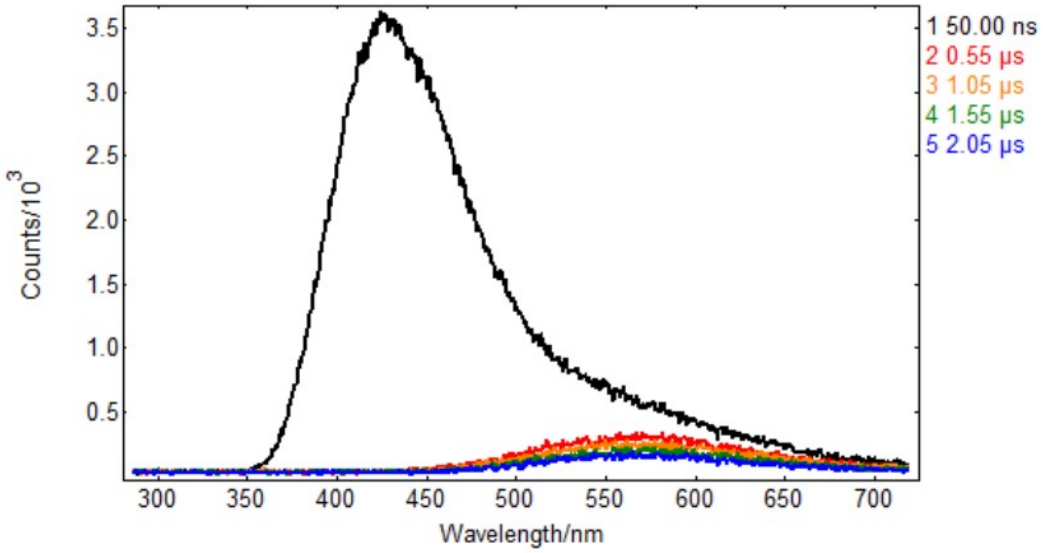

Figure S49. LIF spectra of BT2O4Cz acquired at 77K in LP980 at varying delays after the pump pulse (colour coding in the graph). Measurement conditions: λ exc = 355 nm, Spectrograph bandwidth = 2 nm, ICCD gate width = 1 µs, 15 averages / point.

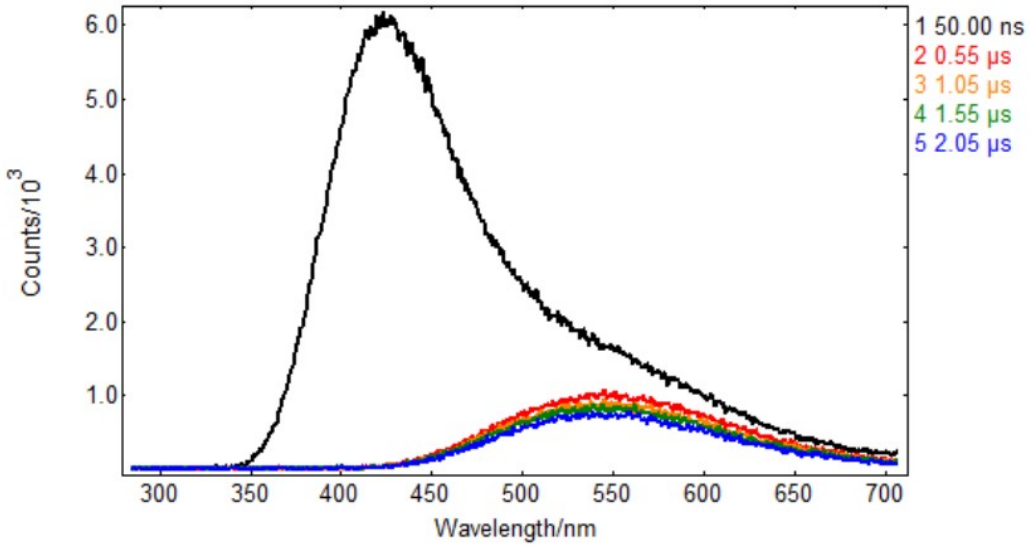

Figure S50. LIF spectra of BT2O4Cz acquired at room temperature in LP980 at varying delays after the pump pulse (colour coding in the graph). Measurement conditions: λ exc = 355 nm, Spectrograph bandwidth = 2 nm, ICCD gate width = 1 µs, 15 averages / point.

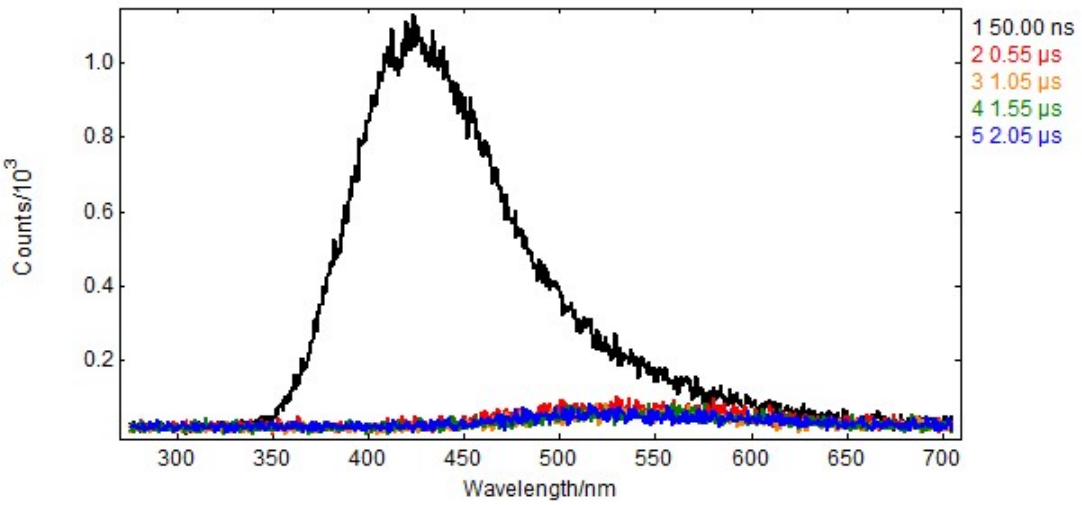

Figure S51. LIF spectra of BT2O6Cz acquired at 77K in LP980 at varying delays after the pump pulse (colour coding in the graph). Measurement conditions: λ exc = 355 nm, Spectrograph bandwidth = 2 nm, ICCD gate width = 1 µs, 15 averages / point.

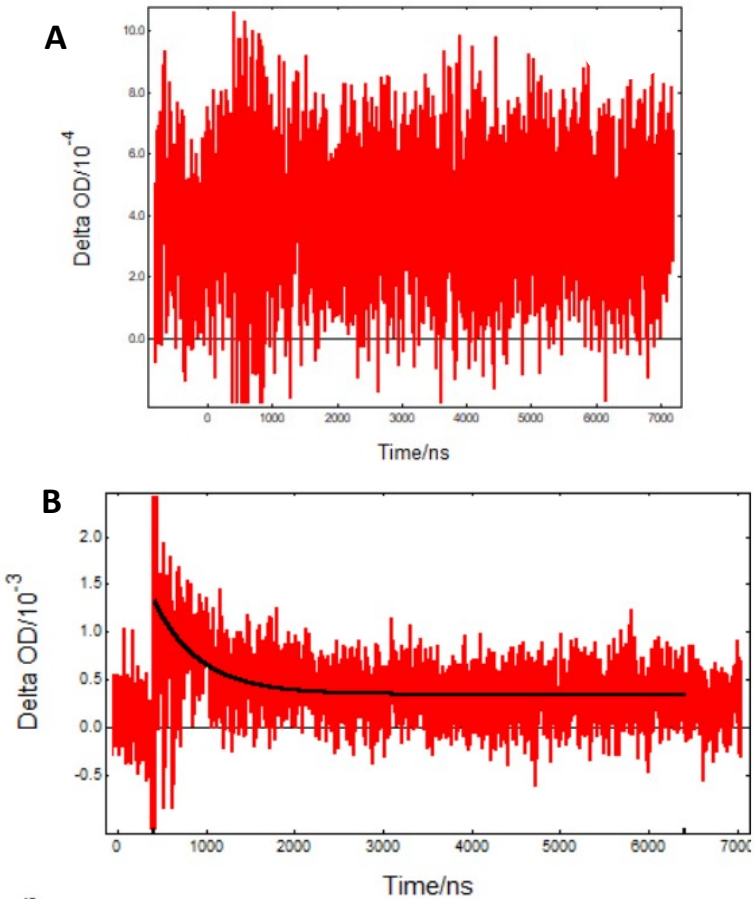

Figure S52. Kinetic TA traces of BT2O4Cz at 550 nm measured at (A) 77K and (B) room temperature. Measurement conditions: λ pump = 355 nm, Spectrograph bandwidth = 1.20 nm, 800 averages.

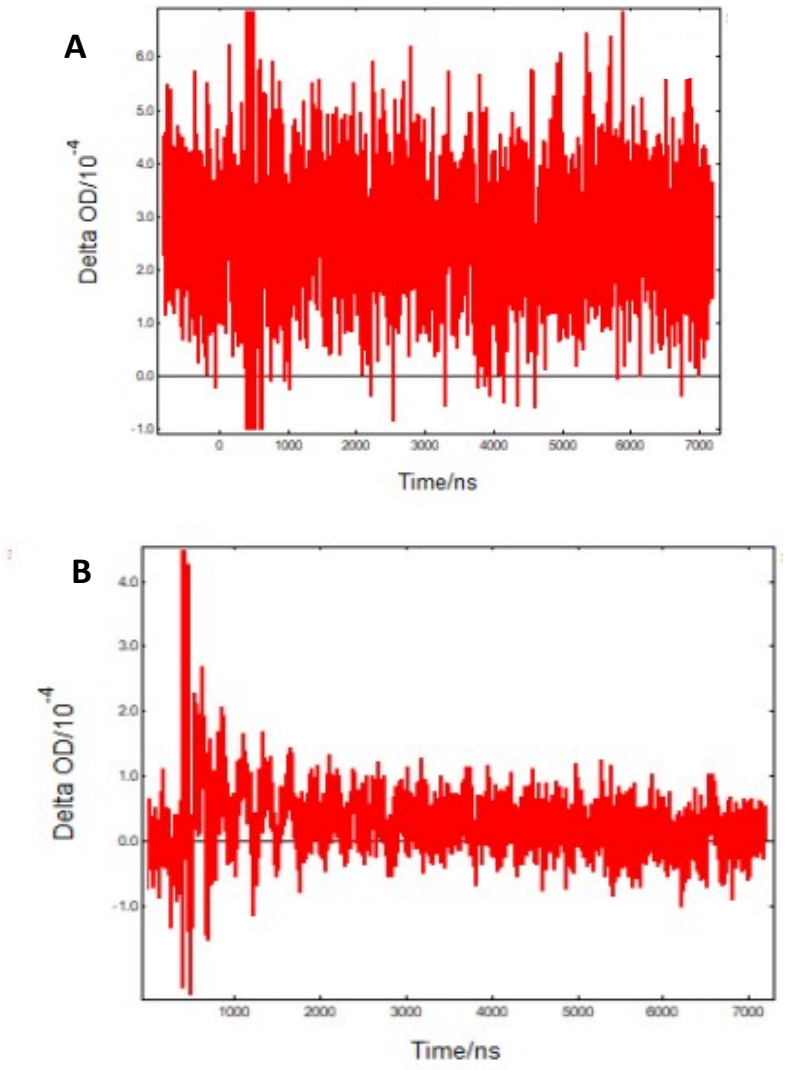

Figure S53. Kinetic TA traces of BT2O6Cz at 550 nm measured at (A) 77K and (B) Room temperature. Measurement conditions: λ pump = 355 nm, Spectrograph bandwidth = 1.20 nm, 800 averages.

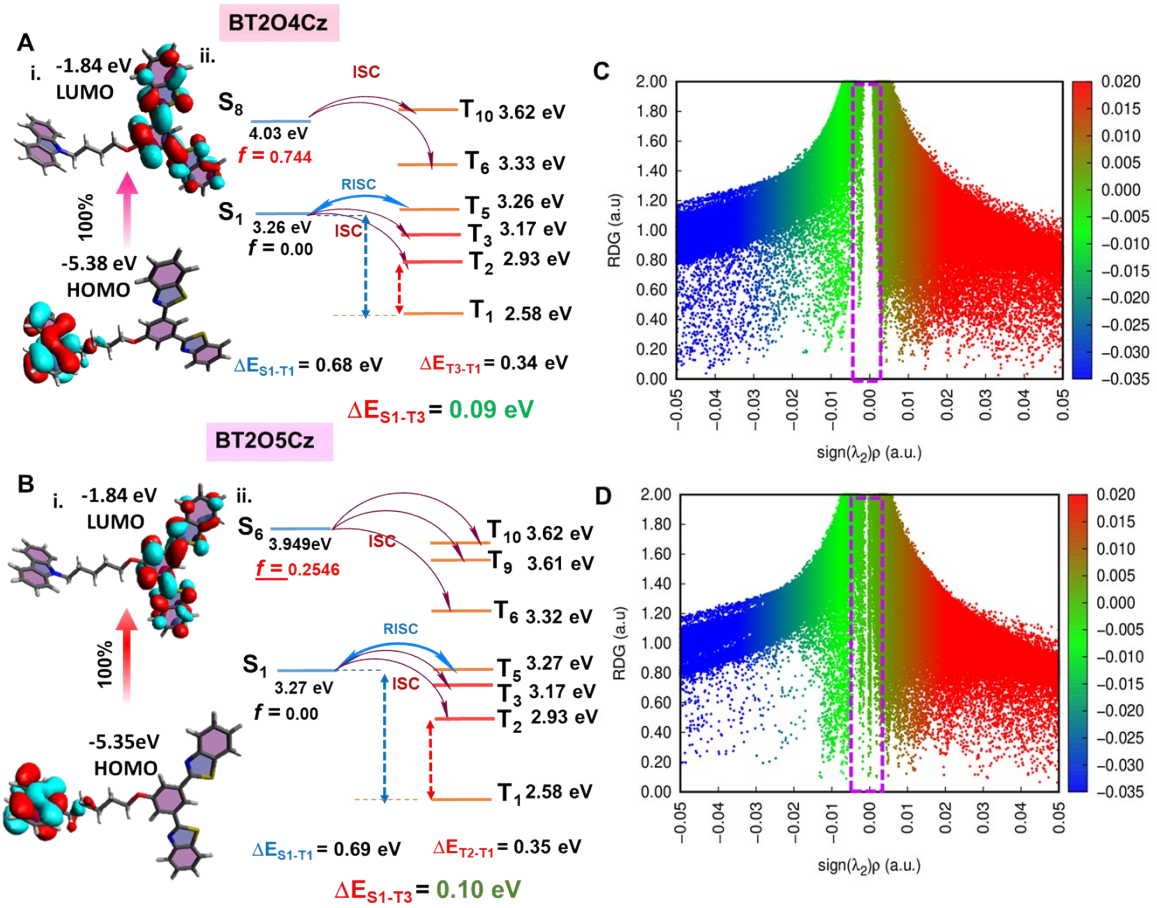

Figure S54. Computational calculations: (Ai and Bi) HOMO and LUMO density distributions with the corresponding band gap profiles, (Aii and Bii) TDDFT energy transitions dependent oscillator strength (*f*) and possible manifold active ISC channels and energy splitting (ΔE_{ST}) for BT2O4Cz and BT2O5Cz from Gaussian 16 package at B3LYP-6-31G(d,p) level of theory. (C and D) The functions of reduced density gradient (RDG) and Sign (λ_2)ρ isosurface map with an isovalue of 0.5 for BT2O4Cz and BT2O5Cz respectively.

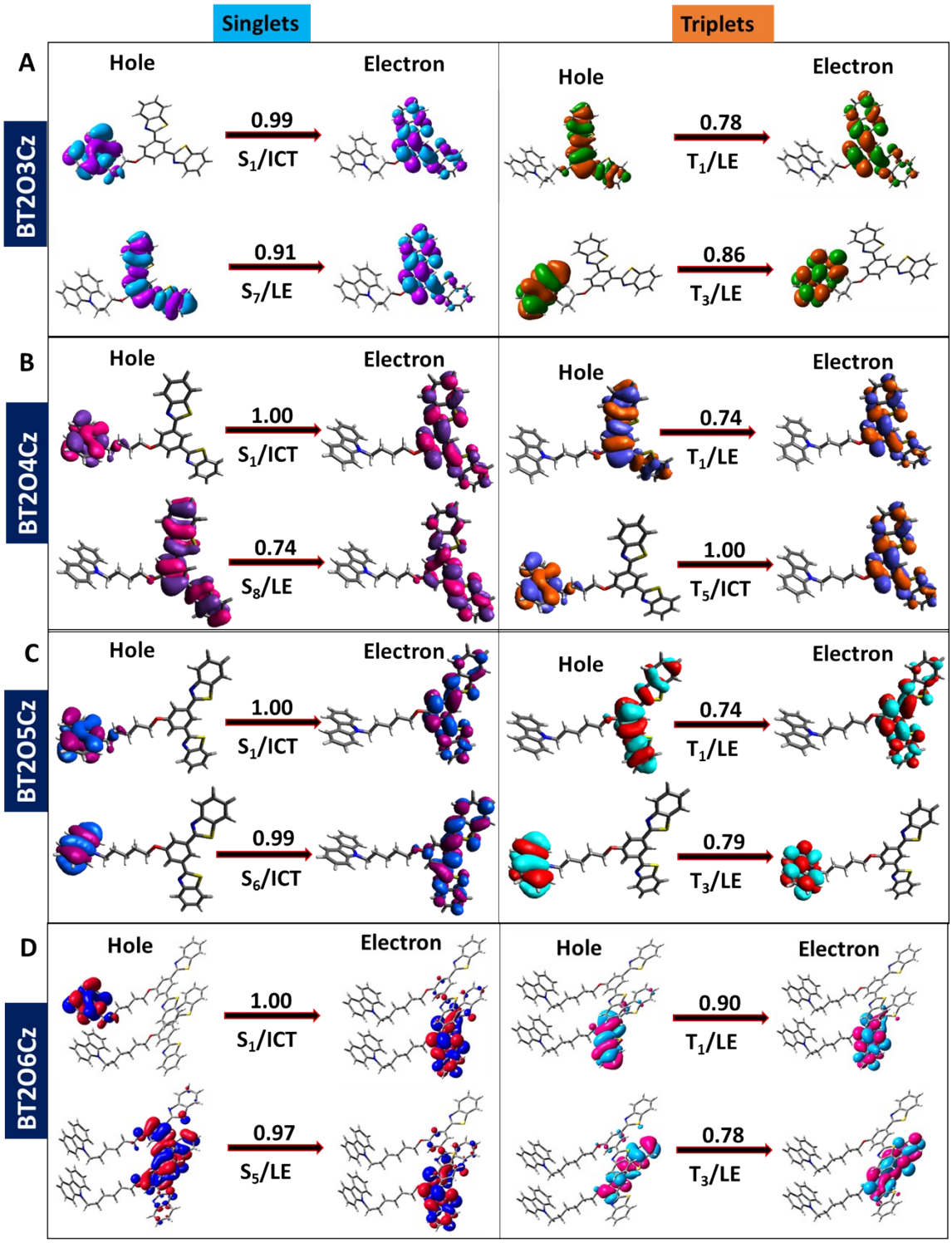

Figure S55. Natural transition orbitals (NTOs) for different singlet and triplet excited states in BT2OxCz (x=3,4,5,6).

Table S2. Adiabatic energy transitions with major frontier orbital contribution for BT2O3CZ at B3LYP/6-31G (d,p) level for singlet states.

State	Energy (eV)	Energy (cm^{-1})	Wavelength (nm)	Osc. Strength	Symmetry	Major contributions
S_1	3.24	26203.34029	381.6307345	0.0002	HOMO→LUMO	100%
S_2	3.58	28913.36317	345.8608375	0	H-1→LUMO	100%
S_3	3.63	29342.45013	340.8031694	0	HOMO→L+1	100%
S_4	3.82	30888.61497	323.7438781	0.1019	H-3→LUMO	55%
S_5	3.96	32016.17806	312.342091	0	H-1→L+1	100%
S_6	4.06	32805.79485	304.8241948	0.0447	HOMO→L+2	88%
S_7	4.11	33190.52131	301.2908386	0.2039	H-3→LUMO	22%
S_8	4.20	33914.00063	294.8634727	0.6071	H-3→LUMO	17%
S_9	4.26	34436.6479	290.3883104	0.0501	H-5→LUMO	21%
S_{10}	4.29	34612.47677	288.9131589	0.3902	H-5→LUMO	53%

Table S3. Adiabatic energy transitions with major frontier orbital contribution for BT2O3CZ at B3LYP/6-31G (d,p) level for triplet states.

State	Energy (eV)	Energy (cm^{-1})	Wavelength (nm)	Osc. Strength	Symmetry	Major contributions
T_1	2.74	22172.18125	451.0156166	0	H-2→LUMO	66%
T_2	3.12	25170.95062	397.2833665	0	H-3→LUMO	33%
T_3	3.22	26011.38034	384.4471101	0	H-1→L+2	77%
T_4	3.24	26193.66164	381.7717484	0	HOMO→LUMO	98%
T_5	3.33	26935.69171	371.2546204	0	H-6→LUMO	14%
T_6	3.38	27288.96255	366.4485222	0	HOMO→L+2	90%
T_7	3.54	28587.51518	349.8030499	0	H-5→LUMO	21%

T_8	3.58	28914.16973	345.8511897	0	H-1→LUMO	100%
T_9	3.60	29057.73641	344.1424293	0	H-4→L+1	13%
T_{10}	3.64	29358.58122	340.6159149	0	HOMO→L+1	95%

Table S4. Adiabatic energy transitions with major frontier orbital contribution for BT2O4CZ at B3LYP/6-31G (d,p) level for singlet states.

State	Energy (eV)	Energy (cm^{-1})	Wavelength (nm)	Osc. Strength	Symmetry	Major contributions
S_1	3.26	26334.81	379.7256	0	HOMO→LUMO	100%
S_2	3.62	29270.67	341.639	0.0001	H-1→LUMO	100%
S_3	3.62	29274.7	341.5919	0	HOMO→L+1	100%
S_4	3.69	29807.83	335.4823	0.1066	H-3→LUMO	76%
S_5	3.94	31833.09	314.1385	0.2077	H-2→LUMO	86%
S_6	3.99	32185.55	310.6984	0	H-1→L+1	100%
S_7	4.02	32476.72	307.9129	0.0737	HOMO→L+2	91%
S_8	4.03	32573.51	306.998	0.7448	H-3→LUMO	14%
S_9	4.11	33160.68	301.562	0.0437	H-5→LUMO	20%
S_{10}	4.14	33407.48	299.3341	0.3134	H-5→LUMO	60%

Table S5. Adiabatic energy transitions with major frontier orbital contribution for BT2O4CZ at B3LYP/6-31G (d,p) level for triplet states.

State	Energy (eV)	Energy (cm^{-1})	Wavelength (nm)	Osc. Strength	Symmetry	Major contributions
T_1	2.74	22172.18125	451.0156166	0	H-2→LUMO	66%
T_2	3.12	25170.95062	397.2833665	0	H-3→LUMO	33%

T_3	3.22	26011.38034	384.4471101	0	H-1→L+2	77%
T_4	3.24	26193.66164	381.7717484	0	HOMO→LUMO	98%
T_5	3.33	26935.69171	371.2546204	0	H-6→LUMO	14%
T_6	3.38	27288.96255	366.4485222	0	HOMO→L+2	90%
T_7	3.54	28587.51518	349.8030499	0	H-5→LUMO	21%
T_8	3.58	28914.16973	345.8511897	0	H-1→LUMO	100%
T_9	3.60	29057.73641	344.1424293	0	H-4→L+1	13%
T_{10}	3.64	29358.58122	340.6159149	0	HOMO→L+1	95%

Table S6. Adiabatic energy transitions with major frontier orbital contribution for BT2O5CZ at B3LYP/6-31G (d,p) level for singlet states.

State	Energy (eV)	Energy (cm^{-1})	Wavelength (nm)	Osc. Strength	Symmetry	Major contributions
S_1	3.27	26292.87	380.3313	0	HOMO→LUMO	100%
S_2	3.62	29058.54	344.1329	0	HOMO→L+1	100%
S_3	3.63	29594.9	337.896	0	H-1→LUMO	100%
S_4	3.69	30299.02	330.0436	0.0869	H-3→LUMO	60%
S_5	3.94	32335.57	309.2569	0	H-1→L+1	100%
S_6	3.99	32731.59	305.5152	0.2546	H-3→LUMO	15%
S_7	4.01	33144.55	301.7087	0.0813	HOMO→L+2	90%
S_8	4.04	33367.96	299.6887	0.6491	H-3→LUMO	21%
S_9	4.11	33986.59	294.2337	0.0565	H-5→LUMO	13%
S_{10}	4.15	34306.79	291.4875	0.3984	H-5→LUMO	51%

Table S7. Adiabatic energy transitions with major frontier orbital contribution for BT2O5CZ at B3LYP/6-31G (d,p) level for triplet states.

State	Energy (eV)	Energy (cm^{-1})	Wavelength (nm)	Osc. Strength	Symmetry	Major contributions
T_1	2.58	20841.36645	479.8149884	0	H-3→L+1	15%
T_2	2.93	23654.62829	422.750249	0	H-3→LUMO	35%
T_3	3.17	25572.61473	391.0433136	0	H-1→L+2	74%
T_4	3.21	25914.5938	385.8829537	0	H-6→LUMO	18%
T_5	3.27	26379.16915	379.0869963	0	HOMO→LUMO	100%
T_6	3.32	26834.87241	372.6494335	0	HOMO→L+2	93%
T_7	3.41	27547.05997	363.0151461	0	H-5→LUMO	12%
T_8	3.45	27841.45233	359.1766651	0	H-4→LUMO	12%
T_9	3.61	29181.13924	342.6871006	0	H-6→LUMO	21%
T_{10}	3.62	29263.40779	341.7237005	0	HOMO→L+1	100%

Table S8. Adiabatic energy transitions with major frontier orbital contribution for BT2O6CZ at B3LYP/6-31G(d,p) level for singlet states.

State	Energy (eV)	Energy (cm^{-1})	Wavelength (nm)	Osc. Strength	Symmetry	Major contributions
S_1	3.29	26557.41768	376.5426337	0	HOMO→LUMO	100%
S_2	3.64	29398.10238	340.1580099	0	HOMO→L+1	100%
S_3	3.66	29540.86252	338.5141512	0	H-1→LUMO	100%
S_4	3.68	29754.59944	336.0824944	0.1053	H-3→LUMO	75%
S_5	3.94	31855.67373	313.9158219	0.2169	H-2→ LUMO	85%
S_6	4.01	32369.4489	308.9332794	0	H-1→L+1	100%

S_7	4.01	32383.16032	308.8024733	0.0486	HOMO→L+2	92%
S_8	4.03	32582.37927	306.9143575	0.7802	H-3→LUMO	14%
S_9	4.11	33205.84584	301.1517926	0.0402	H-5→LUMO	16%
S_{10}	4.15	33482.49401	298.6635343	0.296	H-5→LUMO	62%

Table S9. Adiabatic energy transitions with major frontier orbital contribution for BT2O6CZ at B3LYP/6-31G(d,p) level for triplet states.

State	Energy (eV)	Energy (cm^{-1})	Wavelength (nm)	Osc. Strength	Symmetry	Major contributions
T_1	2.58	20842.173	479.7964205	0	H-3→L+1	14%
T_2	2.93	23652.20863	422.7934971	0	H-3→LUMO	35%
T_3	3.17	25575.84094	390.9939862	0	H-1→L+2	74%
T_4	3.20	25870.23331	386.5446392	0	H-6→LUMO	18%
T_5	3.29	26557.41768	376.5426337	0	HOMO→LUMO	100%
T_6	3.32	26796.96435	373.1765983	0	HOMO→L+2	93%
T_7	3.41	27520.44367	363.3662349	0	H-5→LUMO	11%
T_8	3.45	27846.29166	359.1142448	0	H-5→LUMO	10%
T_9	3.61	29186.78512	342.6208114	0	H-6→LUMO	21%
T_{10}	3.64	29398.10238	340.1580099	0	HOMO→L+1	100%

Table S10. Crystallographic data and structure refinement parameters of BT2O3Cz and BT2O6Cz crystal.

Compound	**BT2O3Cz**	**BT2O6Cz**
Empirical formula	C35 H25 N3 O S2	C38 H31 N3 O S2
CCDC NO	1969742	1969743
Temperature/K	296	293
Crystal system	monoclinic	orthorhombic
Space group	P 21/c	P c a 21
a/Å	5.737(5)	40.9226(8)
b/Å	19.159(18)	6.2134(1)
c/Å	24.68(2)	11.8600(2)
α/°	90.00	90.00
β/°	96.66(3)	90.00
γ/°	90.00	90.00
Volume/Å^3	2694(4)	3015.63(9)
Z	4	4
ρ_{calc}mg/mm^3	1.400	1.343
m/mm^{-1}	0.234	1.883
F(000)	1184.0	1280.0
Index ranges	-6≤ h ≤ 6, -22 ≤ k ≤ 22, -29 ≤ l ≤ 29	-48 ≤ h ≤ 48, -7 ≤ k ≤ 7, -14 ≤ l ≤ 14
Reflections collected	94738	18331
Independent reflections	4760	5301[2794]
Data/restraints/parameters	4760/0/370	5301/0/397
Goodness-of-fit on F^2	1.045	1.014
Final R indexes	R1 = 0.0850, wR2 = 0.2065	R1 = 0.0547, wR2 = 0.1278

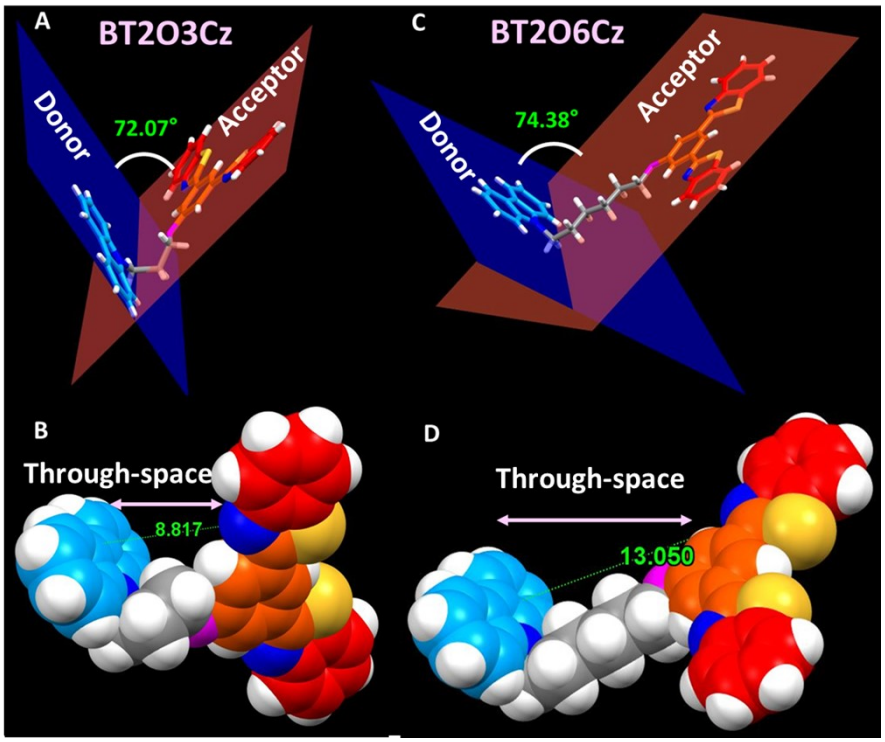

Figure S56. SC-XRD analysis: (A-D) Narrow/wider angle and short/long through-space distance between donor-acceptor planes in the single-crystal XRD structure for BT2O3Cz and BT2O6Cz OSMWLEs.

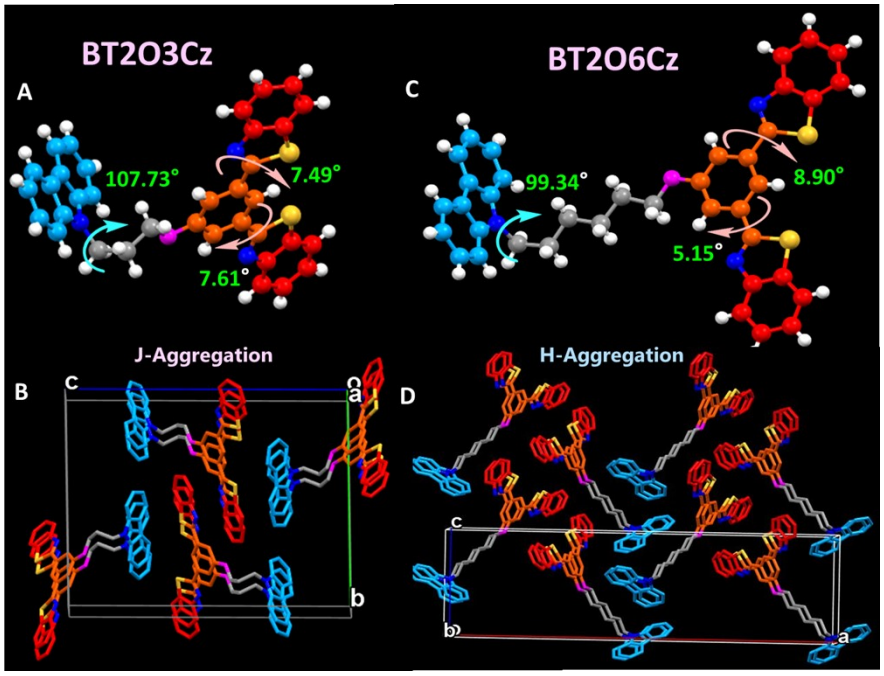

Figure S57. SC-XRD analysis: (A and B) Dihedral angles and type of dimeric assembly for BT2O3Cz and BT2O6Cz OSMWLEs in unit cell.

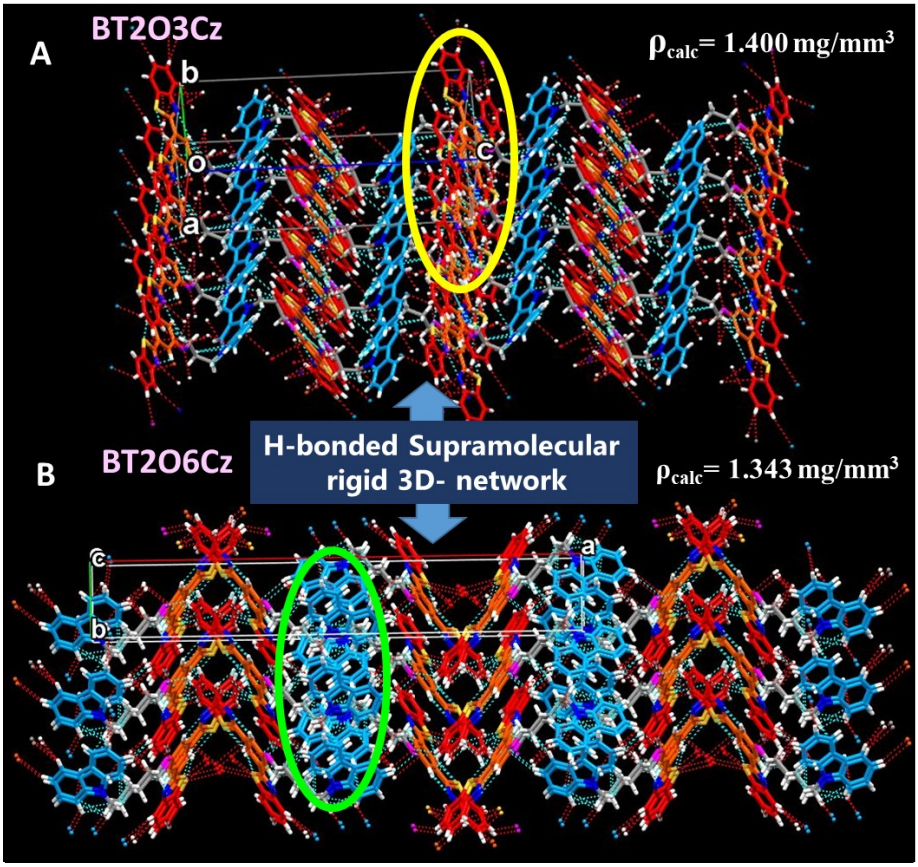

Figure S58. SC-XRD analysis: (A and B) H-bonded supramolecular rigid 3D- crystal packing for BT2O3Cz and BT2O6Cz in bulk. BT2O3Cz showed large π-core containing acceptor stacking (yellow circle) which is comparatively higher dense packing (ρ_{cal} = 1.400 mg/mm^3) than donor based π-staking (green circle) showed ρ_{cal} = 1.343 mg/mm^3 in BT2O6Cz.

Table S11. Summarized table of SCXRD-crystal structural analysis with non covalent interactions, dihedral and slip angle informations.

Single Crystals	Intra-molecular Interactions Close contact distance (Å)					Intermolecular Interactions Close contact distance (Å)					Sweep Angle (Degree)		
	CH-S	CH-N	CH-π	π-CH	BT $_{π-π}$	CZ_{CH} $_{-π}$	CH-O	CH-N	CH-π	π-S	BT-BT	Ph-Ph	Cz-Cz
BT2O3Cz	2.743	2.556	2.834	2.726	3.351	-	2.705	2.663	2.792	-	96.19	51.91	47.75
BT2O6Cz	2.643	2.575	2.808	2.752	3.369	2.853 2.888	2.645	-	2.869	3.310	42.03	37.74	137.86

Table S12. Calculated attachment energies of different crystal facets for BT2O3Cz.

hkl	Dhkl/Å	Eatt(Total)/kcal mol^{-1}	Eatt(vdW)/kcal mol^{-1}	% Total facet area
{ 0 1 1 }	15.09541	-73.40388503	-70.00425858	50.61294073
{ 0 0 2 }	12.25673	-59.41677538	-59.91612851	31.19920067
{ 1 0 0 }	5.698286	-169.7176518	-155.2817056	6.91903336
{ 1 1 -1 }	5.461538	-172.7664881	-161.2503639	5.36009409

Table S13. Calculated attachment energies of different crystal facets for BT2O6Cz.

hkl	Dhkl/Å	Eatt(Total)/kcal mol^{-1}	Eatt(vdW)/kcal mol^{-1}	% Total facet area
{ 2 0 0}	20.4613	-55.3638598	-48.23128222	52.38292617
{ 2 0 1}	10.26091359	-123.5714912	-108.106391	14.0966025
{ 2 0 -1}	10.26091359	-123.5714912	-108.106391	14.0966025
{ 0 1 0}	6.2134	-177.4611538	-168.3216253	14.36666498

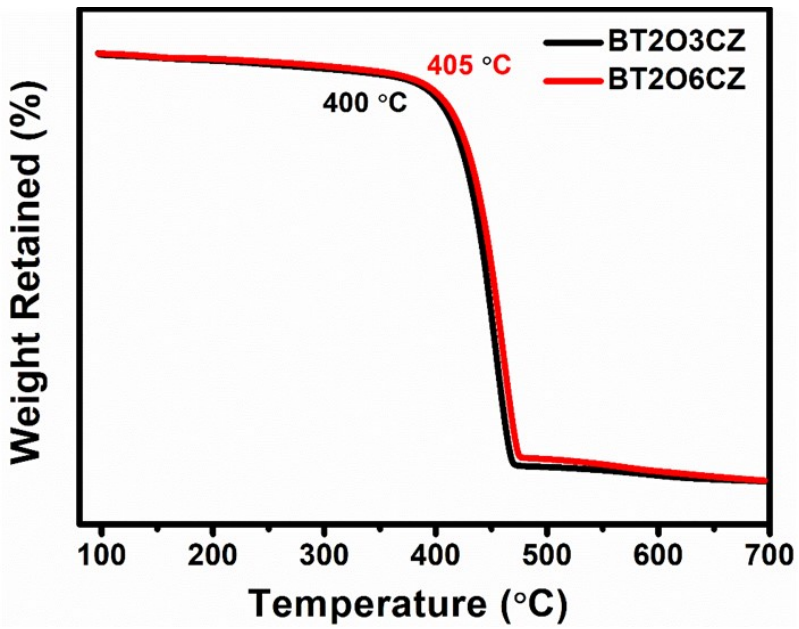

Figure S59. Thermogravimetric analysis (TGA) to investigate thermal stability for the short and long chain BT2O3Cz and BT2O6Cz emitters.

References

[1] G. M. Sheldrick, *Acta Cryst.* C71, **2015**, 3.

[2] Material Studio 8.0, Acceryls Inc., San Diego, **2014**.

[3] S. K. Wolff, D. J. Grimwood, A. J. McKinnon, J. J. Wolff, M. J. Turner, D. Jayatilaka, M. A. Spackman, CrystalExplorer 3.1; University of Western Australia, **2012**.

[4] M. A. Spackman, D. Jayatilaka, *Cryst. Eng. Comm*. **2009**, *11*, 19.

[5] J. M. Spackman, A. J. McKinnon, D. Jayatilaka, *Cryst. Eng. Comm.* **2008**, *10*, 377.

[6] T. Petrenko, S. Kossmann, F. Neese, *J. Chem. Phys.* **2011**, *134*, 054116.

[7] B. de Souza, F. Neese, R. Izsák, *J. Phys. Chem.* **2018**, *148*, 034104.

[8] B. de Souza, G. Farias, F. Neese, R. Izsák, *J. Chem. Theo. Comp.* **2019**, *15*, 1896.

[9] K. Masui, H. Nakanotani, C. Adachi, *Org. Electron*. **2013**, *14*, 2721.

[10] C. S. McCamy, *Color Res. Appl.* **1992**, *17*. 142-144

[11] Q. Gao, X. Wu, F. Jia, M. Liu, Y. Zhu, Q. Cai, A. Wu, *J. Org. Chem.* **2013**, *78*, 2792.